



# The in-plane mechanical properties of highly compressible and stretchable 2D lattices



S. Adhikari \*

Future Manufacturing Research Institute, College of Engineering, Swansea University, Swansea, UK

## ARTICLE INFO

### Keywords:

Hexagonal lattices  
Stiffness matrix  
Homogeneous properties  
Elastic constants  
2D materials  
Nonlinear analysis

## ABSTRACT

Highly compressible and stretchable lattice materials are perfectly suitable to be exploited in a range of cutting edge engineering applications such as low band-gap acoustic metamaterials, vibration absorbers, soft robotics, stretchable electronics and stent devices. Physics-based understanding and efficient computational methods are of paramount importance for the analysis and design of such cellular metamaterials. This paper develops the analytical framework to understand the nonlinear mechanics of hexagonal lattices subject to in-plane compressive and tensile stresses. Nonlinear equivalent elastic moduli and Poisson's ratios of the stressed lattice are expressed through the coefficients of the stiffness matrices of the constitutive beam elements. The stiffness coefficients, in turn, are derived from the transcendental displacement function which is the exact solution of the corresponding governing ordinary differential equation with appropriate boundary conditions. The closed-form analytical expressions of the equivalent elastic properties of the lattice are expressed in terms of trigonometric functions for the case of compressive stress and hyperbolic functions for the case of tensile stress. The general expressions are then used to investigate three special cases of wide interest, namely, auxetic hexagonal lattices, rhombus-shaped lattices and rectangular lattices. Analytical expressions are validated using independent nonlinear finite element simulation results. Numerical results are displayed for applied compressions and tensions in both directions separately and together. The equivalent elastic moduli show a softening effect under compression and a stiffening effect under tension. The Poisson's ratios are not significantly affected by the applied stresses. The proposed analytical approach and the new closed-form expressions provide a computationally efficient and physically intuitive framework for the analysis and parametric design of lattice materials under external stresses.

## 1. Introduction

Hexagonal lattices, commonly known as honeycombs, are widely used in engineering structures across different length scales. Cellular solids in general, and hexagonal lattices in particular, have several desirable properties. They include but are not limited to, excellent strength to weight ratio, outstanding energy absorption and impact resistance and the ability to withstand crushing and other transient forces. We refer to the book by Gibson and Ashby [1] and an insightful review paper by Fleck et. al. [2] for a general introduction to cellular solids, an overview of analytical methods and experimental results in the field. The mechanics of hexagonal lattices plays a key role in understanding nanoscale material systems such as single-layer graphene [3], bilayer graphene [4], boron nitride nanosheets [5] and more complex multilayer nano-heterostructures [6]. Recent develop-

ments in mechanical metamaterials, such as pentamode materials [7,8], additive layer manufacturing (3D printing) and multiphysics applications involving, thermal, magnetic, electromechanical and piezoelectric phenomenon demands an advanced understanding of cellular materials than ever before.

Honeycombs and other cellular materials are made of periodic unit cells. When the number of cells is sufficiently large, cellular materials can be effectively modelled as a continuum with equivalent elastic properties. Such equivalent properties can be derived from the mechanics of a unit cell. This approach is not only computationally efficient but also physically insightful [9–15]. We refer to a recent review paper [16] for further discussions. When the cellular material is not perfectly periodic, a representative unit cell approach was recently developed [17] to generalise the classical unit cell formulation to obtain equivalent elastic moduli. While these unit cell-based

\* Corresponding author.

E-mail address: [S.Adhikari@swansea.ac.uk](mailto:S.Adhikari@swansea.ac.uk)

methods can be efficient in obtaining overall linear elastic properties, the analysis of buckling and other instabilities is more challenging due to the need to consider inherent nonlinearities. Experimental and computational approaches for a comprehensive understanding of crushing and buckling behaviour of honeycombs was developed in [18]. Instability analysis of metallic hexagonal lattices under general in-plane loads was conducted using theoretical approaches by [19]. On the other hand, reference [20] considered transverse loading for theoretical analysis of elastoplastic yielding and curing. Since these earlier works, several authors (see for example [21–26]) have considered numerical, theoretical and experimental studies on crushing, buckling, instability analysis and general response characterisation of cellular materials under compressive loading. Zhang et al. [27] considered initial yield surfaces of lattice structures along with equivalent elastic properties. Amendola and Fraternali [28] proposed analytical formulations for response analysis of 2D and 3D auxetic composite lattices under isotropic prestress. In-plane crashworthiness of re-entrant honeycomb structures was investigated using nonlinear finite element analysis in [29]. Non-linear finite element analysis was used in [30] for in-plane dynamic crushing of circular-celled honeycomb structures. Homogenised properties of honeycombs under axial and shear loading are considered in [31,32]. Effective elastic properties of flexible hexagonal honeycombs with geometric nonlinearities and large deformations are considered in [33–35].

From this brief literature review, it is evident that extensive research has been conducted on the large deformation of lattice materials leading to nonlinear stress-strain relationships. Another situation when nonlinear behaviour is of paramount importance is when highly-stretchable and soft lattices are considered [36–40]. They are useful for many practical applications such as impact absorption, biological metamaterials, soft robots, stretchable electronics and fashion/architecture. Such highly-stretchable lattices can be realised through 3D printing, for example, SLA or FDM with flexible materials such as TPU and TPE. Computational and experimental works have provided an excellent physical understanding of the mechanisms underpinning nonlinear behaviour. However, a direct and simple analytical quantification of the underlying nonlinear relationship for a general 2D lattice structure has remained an open problem. Our aim in this paper is to obtain a nonlinear stress-strain relationship using homogeneous equivalent elastic moduli of the lattice. For two-dimensional lattices, the equivalent in-plane elastic properties are quantified by two equivalent elastic moduli for the two orthogonal directions along with two Poisson's ratios and the shear modulus. It is assumed that the lattice is perfectly periodic. Although geometric nonlinearities are considered, linear elastic material behaviour is assumed.

The paper is organised as follows. In Section 2, the elasticity tensor of 2D lattices and the unit cell approach to obtain the equivalent elastic properties are discussed. The equivalent elastic properties investigated include elastic moduli in both directions, Poisson's ratio for both directions and the shear modulus. Further details about the physics-based method underpinning the expression of the equivalent elastic properties are given in the supplementary document. Closed-form expressions of the elements of the elasticity tensor are given in terms of the coefficients of the stiffness matrix of the beams within the unit cell. The stiffness matrix of Euler-Bernoulli beams considering axial forcing is derived in Section 3. Three cases are considered, (a) stiffness matrix obtained using the classical finite element method, (b) exact stiffness matrix with compressive axial force, and (c) exact stiffness matrix with tensile axial force. The stiffness coefficients derived here are utilised in the expression of equivalent elastic properties of the lattice. In Section 4, hexagonal lattices undergoing compressive stress is discussed. Three separate scenarios have been considered, namely, compressive stress only along direction 1, compressive stress only along direction 2 and compressive stresses along with both directions. Hexagonal lattices undergoing tensile stress are in discussed in Section 5. Again three different scenarios have been considered,

namely, tensile stress only along direction 1, tensile stress only along direction 2 and tensile stresses along with both directions. The general analytical framework for the equivalent elastic properties of stressed hexagonal lattices has been applied to different lattice geometries in Section 6. The special cases investigated include auxetic hexagonal lattices, rhombus-shaped lattices and rectangular lattices. Exact closed-form expressions of all the five equivalent elastic constants have been explicitly derived. Finally, in Section 7 some conclusions are drawn based on the results obtained in the paper.

## 2. Equivalent elastic moduli of hexagonal lattices

### 2.1. The elasticity tensor of 2D lattices

The effective elastic properties of a lattice material is important for global stress-strain analysis. When in-plane elasticity of 2D materials are considered, the constitutive relationship can be expressed as

$$\begin{Bmatrix} \varepsilon_{11} \\ \varepsilon_{22} \\ 2\varepsilon_{12} \end{Bmatrix} = \begin{bmatrix} 1/E_1 & -\nu_{21}/E_2 & 0 \\ -\nu_{12}/E_1 & 1/E_2 & 0 \\ 0 & 0 & 1/G_{12} \end{bmatrix} \begin{Bmatrix} \sigma_{11} \\ \sigma_{22} \\ \sigma_{12} \end{Bmatrix} \quad (1)$$

This is based on the fact that the material is orthotropic [41]. Here  $\varepsilon_{(\bullet)}$  and  $\sigma_{(\bullet)}$  represent strain and stress within the 2D material. In the above equation  $E_1$  is the longitudinal Young's modulus,  $E_2$  is the transverse Young's modulus,  $G_{12}$  is the shear modulus,  $\nu_{12}$  and  $\nu_{21}$  are the Poisson's ratios. These five quantities explicitly define stress-strain relationship. This can be illustrated by inverting the coefficient matrix in Eq. (1) as

$$\begin{Bmatrix} \sigma_{11} \\ \sigma_{22} \\ \sigma_{12} \end{Bmatrix} = \begin{bmatrix} E_1/(1-\nu_{12}\nu_{21}) & \nu_{21}E_1/(1-\nu_{12}\nu_{21}) & 0 \\ \nu_{12}E_2/(1-\nu_{12}\nu_{21}) & E_2/(1-\nu_{12}\nu_{21}) & 0 \\ 0 & 0 & G_{12} \end{bmatrix} \begin{Bmatrix} \varepsilon_{11} \\ \varepsilon_{22} \\ 2\varepsilon_{12} \end{Bmatrix} \quad (2)$$

We consider the case when the external stress applied to the material is large such that it alters the elastic constants. We assume linear material behaviour, but consider geometric nonlinearity arising due to the large deformation. From Eq. (2) we can therefore obtain

$$\begin{aligned} \sigma_{11}(\mu) &= \frac{E_1(\mu)}{(1-\nu_{12}(\mu)\nu_{21}(\mu))} (\varepsilon_{11}(\mu) + \nu_{21}(\mu)\varepsilon_{22}(\mu)) \\ \sigma_{22}(\mu) &= \frac{E_2(\mu)}{(1-\nu_{12}(\mu)\nu_{21}(\mu))} (\nu_{12}(\mu)\varepsilon_{11}(\mu) + \varepsilon_{22}(\mu)) \\ \sigma_{12}(\mu) &= G_{12}(\mu)[2\varepsilon_{12}(\mu)] \end{aligned} \quad (3)$$

In this expression, all the five elasticity constants (three elastic moduli and two Poisson's ratios) are functions of a scalar parameter  $\mu$ . The parameter  $\mu$  symbolically represents externally applied stress to the lattice. The exact expression of  $\mu$  will depend on the nature of the applied stress and will be discussed later. The aim of this paper is to derive analytical expressions of the elasticity constants appearing in Eq. (3). The analysis of complex systems with embedded cellular materials is governed by boundary value problems. In general, some numerical methods such as the finite element method are necessary to solve such problems. The use of stress-dependent elasticity constants will allow coarser discretisation leading to an efficient computational approach. This is possible because stress-dependent elasticity constants take account of nonlinear stress-strain relationship as depicted in Eq. (3).

### 2.2. The unit cell approach

The effective elastic property of a lattice structure can be obtained by exploiting the periodicity of a suitably selected unit cell. In Fig. 1 we show a representative example of a hexagonal lattice and its corresponding unit cell. The unit cell is selected such that it represents the whole lattice under tessellation in both directions. Each of the cell walls will bend and stretch/compress when subjected to in-plane ten-

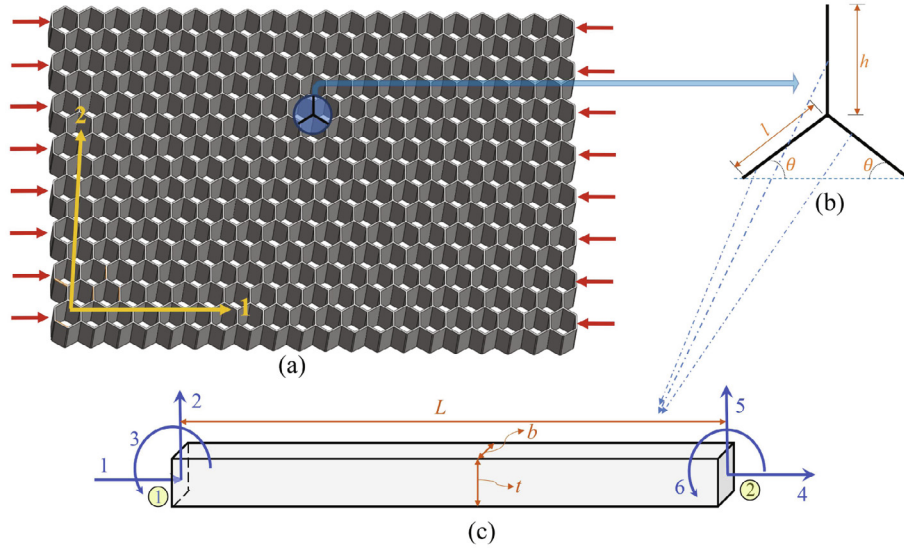


**Fig. 1.** (a) Illustration of a hexagonal lattice subjected to compressive stress in direction-1, (b) The unit cell used to analyse the mechanics of the lattice. It comprised of three beams connected at one point. (c) A beam element (representing each of the three beams in the unit cell model) with six degrees of freedom and two nodes. The degrees of freedom in each node corresponds to the axial, transverse and rotational deformation.

sile/compressive stresses. When the applied stress is uniform along the out-of-plane direction, each element of the unit cell in Fig. 1(b) can be modelled as a beam. In Fig. 1(c) a general beam element with six degrees of freedom and two nodes is shown. The stiffness matrix of the beam element can be expressed by a  $6 \times 6$  matrix with degrees of freedom in each node corresponding to the axial, transverse and rotational deformation. Considering only the bending deformation and ignoring any stretching/shortening deformations, the equivalent elastic moduli of hexagonal cellular materials are obtained by Gibson and Ashby [1] as

$$E_{1GA} = E\alpha^3 \frac{\cos \theta}{(\beta + \sin \theta) \sin^2 \theta} \quad (4)$$

$$E_{2GA} = E\alpha^3 \frac{(\beta + \sin \theta)}{\cos^3 \theta} \quad (5)$$

$$\nu_{12GA} = \frac{\cos^2 \theta}{(\beta + \sin \theta) \sin \theta} \quad (6)$$

$$\nu_{21GA} = \frac{(\beta + \sin \theta) \sin \theta}{\cos^2 \theta} \quad (7)$$

$$\text{and } G_{12GA} = E\alpha^3 \frac{(\beta + \sin \theta)}{\beta^2 (1 + 2\beta) \cos \theta} \quad (8)$$

Here  $E$  is the elastic modulus of the base material,  $\theta$  is the cell angle as shown in Fig. 1(b),  $\alpha$  and  $\beta$  are geometric non-dimensional ratios given by

$$\alpha = \frac{t}{l} \quad (\text{thickness ratio}) \quad (9)$$

$$\text{and } \beta = \frac{h}{l} \quad (\text{height ratio}) \quad (10)$$

The key focus of this paper is to explicitly consider the role of in-plane stress on the elastic behaviour of 2D lattices. In general, a non-linear stress-strain relationship is expected. This, in turn, will be reflected in the elastic constants which are depended on the applied stress as in Eq. (3). When external stress is applied to a cellular material as depicted in Fig. 1(a), it results in forces and moments on the unit cell shown in Fig. 1(b). The deformation of the unit cell due to the applied stress can be obtained using the coefficients of the stiffness matrix of the typical element shown in Fig. 1(c). Following the analytical derivation proposed in the supplementary document, the exact expressions of the five elastic constants are given by

$$E_1(\mu) = \frac{K_{55}(\mu) \cos \theta}{b(\beta + \sin \theta) \sin^2 \theta \left(1 + \cot^2 \theta \frac{K_{55}(\mu)}{K_{44}(\mu)}\right)} \quad (11)$$

$$E_2(\mu) = \frac{K_{55}(\mu) (\beta + \sin \theta)}{b \cos^3 \theta \left(1 + \tan^2 \theta \frac{K_{55}(\mu)}{K_{44}(\mu)} + 2 \sec^2 \theta \frac{K_{55}(\mu)}{K_{44}^{(h)}(\mu)}\right)} \quad (12)$$

$$\nu_{12}(\mu) = \frac{\cos^2 \theta \left(1 - \frac{K_{55}(\mu)}{K_{44}(\mu)}\right)}{(\beta + \sin \theta) \sin \theta \left(1 + \cot^2 \theta \frac{K_{55}(\mu)}{K_{44}(\mu)}\right)} \quad (13)$$

$$\nu_{21}(\mu) = \frac{(\beta + \sin \theta) \sin \theta \left(1 - \frac{K_{55}(\mu)}{K_{44}(\mu)}\right)}{\cos^2 \theta \left(1 + \tan^2 \theta \frac{K_{55}(\mu)}{K_{44}(\mu)} + 2 \sec^2 \theta \frac{K_{55}(\mu)}{K_{44}^{(h)}(\mu)}\right)} \quad (14)$$

$$G_{12}(\mu) = \frac{(\beta + \sin \theta)}{b \cos \theta} \times \frac{1}{\left(-\frac{h^2}{2lK_{65}(\mu)} + \frac{4K_{66}^{(h/2)}(\mu)}{\left(K_{35}^{(h/2)}(\mu)K_{66}^{(h/2)}(\mu) - \left(K_{36}^{(h/2)}(\mu)\right)^2\right)} + \frac{(\cos \theta + (\beta + \sin \theta) \tan \theta)^2}{K_{44}(\mu)}\right)} \quad (15)$$

In the above equations,  $b$  is the depth of the lattice and  $K_{ij}(\mu)$  are the  $ij$ -th element of the stiffness matrix of the beam element shown in Fig. 1(c). It should be noted that in general, the stiffness coefficients are functions of the external stress parameter  $\mu$ . In the next section, we explicitly derive the stiffness coefficients of the beam considering the governing differential equation.

### 3. Stiffness matrices of axially loaded beams

#### 3.1. The classical beam element

When the entire lattice is subjected to compressive or tensile stress, the constitutive beam members also undergo compression or tension. If the axial forces are small, they do not have a significant impact on the bending of the beam. However, if such forces are large, their effect cannot be ignored. We use the Euler-Bernoulli beam theory to characterise the underlying deformation of the beams.



Fig. 2. An Euler–Bernoulli beam subjected to an axial force  $N$ .

A beam with a compressive axial force  $N$  is shown in Fig. 2. The transverse deflection of the beam is governed by the following fourth-order ordinary differential equation

$$EI \frac{d^4 W(x)}{dx^4} + N \frac{d^2 W(x)}{dx^2} = F(x) \quad (16)$$

Here  $W(x)$  and  $F(x)$  are the transverse displacement and applied transverse forcing on the beam. The quantity  $EI$  is the bending stiffness of the beam,  $I$  is the inertia moment of the beam cross section and  $E$  is the Young's modulus of the beam material. The beam element has two nodes and four degrees of freedom. The displacement field within the element is expressed by cubic shape functions [42] for the classical finite element analysis and they are given by

$$\mathbf{N}(\xi) = \left[ 2\xi^3 - 3\xi^2 + 1, L\xi(\xi - 1), -2\xi^3 + 3\xi^2, L\xi^2(\xi - 1) \right]^T \quad (17)$$

In the above, the non-dimensional length variable is expressed as  $\xi = x/L$

Note that these shape functions do not arise from the exact solution of the governing differential Eq. (16) with relevant boundary conditions. Employing these shape functions in conjunction with the conventional variational formulation [42], the stiffness matrix of the general beam element can be obtained as

$$\begin{aligned} \mathcal{K} &= EI \int_0^L \frac{d^2 \mathbf{N}(x)}{dx^2} \frac{d^2 \mathbf{N}^T(x)}{dx^2} dx - N \int_0^L \frac{d\mathbf{N}(x)}{dx} \frac{d\mathbf{N}^T(x)}{dx} dx \\ &= \frac{EI}{L^3} \int_0^1 \frac{d^2 \mathbf{N}(\xi)}{d\xi^2} \frac{d^2 \mathbf{N}^T(\xi)}{d\xi^2} d\xi - \frac{N}{L} \int_0^1 \frac{d\mathbf{N}(\xi)}{d\xi} \frac{d\mathbf{N}^T(\xi)}{d\xi} d\xi \\ &= \frac{EI}{L^3} \int_0^1 \left( \frac{d^2 \mathbf{N}(\xi)}{d\xi^2} \frac{d^2 \mathbf{N}^T(\xi)}{d\xi^2} - \mu^2 \frac{d\mathbf{N}(\xi)}{d\xi} \frac{d\mathbf{N}^T(\xi)}{d\xi} \right) d\xi \end{aligned} \quad (19)$$

In the above equation, the non-dimensional axial force is given by

$$\mu^2 = \frac{NL^2}{EI} \quad (20)$$

Evaluating the integral in Eq. (19) and simplifying we have the classical stiffness matrix of a beam-column corresponding to Fig. 2 as

$$\mathcal{K} = \frac{EI}{L^3} \begin{bmatrix} d_1 & d_2L & -d_1 & d_2L \\ & d_3L^2 & -d_2L & d_4L^2 \\ & & d_1 & -d_2L \\ \text{sym} & & & d_3L^2 \end{bmatrix} \quad (21)$$

where

$$\begin{aligned} d_1 &= 12 - \frac{6}{5}\mu^2, \quad d_2 = 6 - \frac{1}{10}\mu^2, \quad d_3 = 4 - \frac{2}{15}\mu^2, \quad d_4 \\ &= 2 + \frac{1}{30}\mu^2 \end{aligned} \quad (22)$$

If the axial force is tensile in nature, the above equations are also valid if the sign of  $\mu^2$  is changed. Therefore, for the tensile stress, the stiffness matrix coefficients are given by

$$d_1 = 12 + \frac{6}{5}\mu^2, \quad d_2 = 6 + \frac{1}{10}\mu^2, \quad d_3 = 4 + \frac{2}{15}\mu^2, \quad d_4 = 2 - \frac{1}{30}\mu^2 \quad (23)$$

In the absence of the axial force, that is when  $\mu = 0$ , the above expression reduces to the conventional stiffness matrix of Euler–Bernoulli beams as

$$\mathcal{K}_{EB} = \mathcal{K}_{(\mu=0)} = \frac{EI}{L^3} \begin{bmatrix} 12 & 6L & -12 & 6L \\ 6L & 4L^2 & -6L & 2L^2 \\ -12 & -6L & 12 & -6L \\ 6L & 2L^2 & -6L & 4L^2 \end{bmatrix} \quad (24)$$

Although the integral in Eq. (19) is evaluated exactly in deriving the stiffness matrix, the error in employing this matrix in the context of the finite element analysis arises from the fact that the displacement field within the beam is not exactly represented by the cubic polynomials used in the shape function in Eq. (17). As a result, more number of elements needs to be used in solving practical problems. This may be acceptable in a numerical approach, but in order to obtain closed-form analytical expression of the equivalent elastic properties, the exact stiffness matrix of the constituent beams are necessary.

### 3.2. Beams with a compressive force

In contrast to the preceding case, if the stiffness matrix is derived using the exact displacement field, only one 'element' will be necessary for an entire beam (as in the special case with (21) when  $\mu = 0$ ). This in turn will enable us to obtain exact expressions of the elasticity constants of the lattice material. Transforming Eq. (16) in the non-dimensional coordinate  $\xi$  we have

$$\frac{d^4 w(\xi)}{d\xi^4} + \mu^2 \frac{d^2 w(\xi)}{d\xi^2} = 0 \quad (25)$$

Here  $w(\xi) \equiv W(x)$  and the forcing is assumed to be zero. Assuming a solution of the form

$$w(\xi) = \exp[\lambda \xi] \quad (26)$$

and substituting in Eq. (25) results in the characteristics equation

$$\lambda^4 + \mu^2 \lambda^2 = 0 \quad \text{or} \quad \lambda^2(1 + \mu^2) = 0 \quad (27)$$

The four solutions of the above equation are

$$\lambda^2 = 0, \lambda = \pm i\mu \quad \text{or} \quad \lambda_{1,2,3,4} = 0, 0, \pm i\mu \quad (28)$$

Using these solutions, the vector of basis functions is obtained as

$$\mathbf{s}^T(\xi) = \{e^{(0,0,\pm i\mu)\xi}\} = \{1, \xi, \sin \mu \xi, \cos \mu \xi\} \quad (29)$$

Considering these functions, the general solution can be expressed as

$$w(\xi) = \mathbf{s}^T(\xi) \mathbf{c} \quad (30)$$

Here the vector of unknown constants are given by

$$\mathbf{c} = \{c_1, c_2, c_3, c_4\}^T \quad (31)$$

Using the displacement function in Eq. (30), the vector of shape functions are expressed as

$$\mathbf{N}(\xi) = \begin{Bmatrix} N_1(\xi) \\ N_2(\xi) \\ N_3(\xi) \\ N_4(\xi) \end{Bmatrix} = \begin{bmatrix} \mathbf{c}_1^T \\ \mathbf{c}_2^T \\ \mathbf{c}_3^T \\ \mathbf{c}_4^T \end{bmatrix} \mathbf{s}(\xi) \quad (32)$$

Here  $\mathbf{c}_j$  is the vector of constants giving rise to the  $j$ th shape function. These unknown constants need to be obtained from the boundary conditions which define the shape functions. The relationship between the shape functions and the boundary conditions can be represented as in Table 1, where boundary conditions in each column give rise to the corresponding shape function. Writing Eq. (30) for the above four sets of boundary conditions, one obtains

$$\mathcal{A}[\mathbf{c}_1, \mathbf{c}_2, \mathbf{c}_3, \mathbf{c}_4] = \mathbf{I} \quad (33)$$

In the above  $\mathbf{I}$  is a  $4 \times 4$  identity matrix and the matrix  $bcalA$  is identified as

**Table 1**

The relationship between the boundary conditions and the shape functions.

	$N_1(\xi)$	$N_2(\xi)$	$N_3(\xi)$	$N_4(\xi)$
$W(0) = w(0)$	1	0	0	0
$\Theta(0) = \frac{1}{L}w'(0)$	0	1	0	0
$W(L) = w(1)$	0	0	1	0
$\Theta(L) = \frac{1}{L}w'(1)$	0	0	0	1

$$\mathcal{A} = \begin{bmatrix} \mathbf{s}^T(0) \\ \frac{1}{L}\mathbf{s}^T(0) \\ \mathbf{s}^T(1) \\ \frac{1}{L}\mathbf{s}^T(1) \end{bmatrix} = \begin{bmatrix} 1 & 0 & 0 & 1 \\ 0 & L^{-1} & \frac{\mu}{L} & 0 \\ 1 & 1 & \sin(\mu) & \cos(\mu) \\ 0 & L^{-1} & \frac{\mu \cos(\mu)}{L} & -\frac{\mu \sin(\mu)}{L} \end{bmatrix} \quad (34)$$

Solving Eq. (33) for the unknown constants and substituting in Eq. (32) we obtain the exact shape functions as

$$\mathbf{N}(\xi) = [\mathcal{A}^{-1}]^T \mathbf{s}(\xi) = \begin{bmatrix} \frac{\mu \cos(\mu) - \sin(\mu) + \mu}{\mu \cos(\mu) - 2 \sin(\mu) + \mu} & -\frac{\mu \sin(\mu)}{\mu \sin(\mu) + 2 \cos(\mu) - 2} & \frac{\sin(\mu)}{\mu \sin(\mu) + 2 \cos(\mu) - 2} & -\frac{\sin(\mu)}{\mu \cos(\mu) - 2 \sin(\mu) + \mu} \\ -\frac{L(\mu \cos(\mu) - \sin(\mu))}{\mu(\mu \sin(\mu) + 2 \cos(\mu) - 2)} & -\frac{L \sin(\mu)}{\mu \cos(\mu) - 2 \sin(\mu) + \mu} & \frac{L(-\sin(\mu) + \mu(\cos(\mu) + 1))}{\mu(-2 \sin(\mu) + \mu(\cos(\mu) + 1))} & \frac{L(\mu \cos(\mu) - \sin(\mu))}{\mu(\mu \sin(\mu) + 2 \cos(\mu) - 2)} \\ -\frac{\sin(\mu)}{\mu \cos(\mu) - 2 \sin(\mu) + \mu} & \frac{\mu \sin(\mu)}{\mu \sin(\mu) + 2 \cos(\mu) - 2} & -\frac{\sin(\mu)}{\mu \sin(\mu) + 2 \cos(\mu) - 2} & \frac{\sin(\mu)}{\mu \cos(\mu) - 2 \sin(\mu) + \mu} \\ \frac{L(\mu - \sin(\mu))}{\mu(\mu \sin(\mu) + 2 \cos(\mu) - 2)} & -\frac{L \sin(\mu)}{\mu \cos(\mu) - 2 \sin(\mu) + \mu} & \frac{L \sin(\mu)}{\mu(\mu \cos(\mu) - 2 \sin(\mu) + \mu)} & \frac{L(\sin(\mu) - \mu)}{\mu(\mu \sin(\mu) + 2 \cos(\mu) - 2)} \end{bmatrix} \begin{Bmatrix} 1 \\ \xi \\ \sin(\mu\xi) \\ \cos(\mu\xi) \end{Bmatrix} \quad (35)$$

Substituting the exact shape functions in the integral expression of the stiffness matrix in Eq. (19), after some algebraic simplifications we obtain

$$\mathcal{K} = \frac{EI}{L^3} \mathcal{A}^{-1T} \left\{ \int_0^1 \left( \frac{d^2 \mathbf{s}(\xi)}{d\xi^2} \frac{d^2 \mathbf{s}^T(\xi)}{d\xi^2} - \mu^2 \frac{d\mathbf{s}(\xi)}{d\xi} \frac{d\mathbf{s}^T(\xi)}{d\xi} \right) d\xi \right\} \mathcal{A}^{-1} = \frac{EI}{L^3} \begin{bmatrix} d_1 & d_2L & -d_1 & d_2L \\ & d_3L^2 & -d_2L & d_4L^2 \\ & & d_1 & -d_2L \\ \text{sym} & & & d_3L^2 \end{bmatrix} \quad (37)$$

The non dimensional coefficients in the above equation are given by

$$\begin{aligned} d_1 &= -\frac{\mu^3 \sin(\mu)}{\Delta}, & d_2 &= \frac{\mu^2(\cos(\mu) - 1)}{\Delta} \\ d_3 &= \frac{\mu(\mu \cos(\mu) - \sin(\mu))}{\Delta}, & d_4 &= \frac{\mu(\sin(\mu) - \mu)}{\Delta} \end{aligned} \quad (38)$$

and  $\Delta = \mu \sin(\mu) - 2(1 - \cos(\mu))$

The four unique non-dimensional coefficients are functions of the axial force parameter  $\mu$  only. Expanding them in a Taylor series about  $\mu = 0$  results

$$\begin{aligned} d_1 &= 12 - \frac{5}{700}\mu^2 - \frac{1}{63000}\mu^4 - \frac{1}{194040000}\mu^6 - \frac{37}{25225200000}\mu^8 - \frac{59}{50450400000}\mu^{10} + O(\mu^{12}) \\ d_2 &= 6 - \frac{1}{10}\mu^2 - \frac{1}{1400}\mu^4 - \frac{1}{126000}\mu^6 - \frac{37}{388080000}\mu^8 - \frac{59}{50450400000}\mu^{10} + O(\mu^{12}) \\ d_3 &= 4 - \frac{2}{15}\mu^2 - \frac{11}{6300}\mu^4 - \frac{1}{27000}\mu^6 - \frac{509}{582120000}\mu^8 - \frac{14617}{681080400000}\mu^{10} + O(\mu^{12}) \\ d_4 &= 2 + \frac{1}{30}\mu^2 + \frac{13}{12600}\mu^4 + \frac{11}{378000}\mu^6 + \frac{907}{1164240000}\mu^8 + \frac{27641}{136216080000}\mu^{10} + O(\mu^{12}) \end{aligned} \quad (39)$$

Considering only the first term in the above expansion, it can be confirmed that the stiffness matrix in Eq. (37) reduced to the classical stiffness matrix of the Euler-Bernoulli beam [42] given in Eq. (24). If the second term of this expansion is considered, then we obtain the classical tangent stiffness matrix of Euler-Bernoulli beams as derived in Eq. (22). The higher-order terms, therefore, quantify the extended effect of the axial force on the transverse deflection of the beam.

### 3.3. Beams with a tensile force

When the axial force is tensile nature, the equation governing the transverse deflection of the beam can be expressed in the non-dimensional coordinate  $\xi$  as

$$\frac{d^4 w(\xi)}{d\xi^4} - \mu^2 \frac{d^2 w(\xi)}{d\xi^2} = 0 \quad (40)$$

Again assuming a solution of the form  $w(\xi) = \exp[\lambda\xi]$  and substituting in Eq. (40) we obtain the characteristics equation as

$$\lambda^4 - \mu^2 \lambda^2 = 0 \quad \text{or} \quad \lambda^2(1 - \mu^2) = 0 \quad (41)$$

The four solutions of the above equation are

$$\lambda^2 = 0, \lambda = \pm\mu \quad \text{or} \quad \lambda_{1,2,3,4} = 0, 0, \pm\mu \quad (42)$$

Using these solutions, the vector of basis functions is obtained as

---


$$\mathbf{s}^T(\xi) = \{e^{(0,0,\pm\mu)\xi}\} = \{1, \xi, \sinh \mu\xi, \cosh \mu\xi\} \quad (43)$$

Following a procedure similar to the previous section, it can be shown that the stiffness matrix is expressed by Eq. (37). The four stiffness coefficients are now given in terms of hyperbolic functions as

$$\begin{aligned} d_1 &= \frac{\mu^3 \sinh(\mu)}{\Delta}, & d_2 &= \frac{\mu^2(\cosh(\mu) - 1)}{\Delta} \\ d_3 &= \frac{\mu(\mu \cosh(\mu) - \sinh(\mu))}{\Delta}, & d_4 &= \frac{\mu(\sinh(\mu) - \mu)}{\Delta} \end{aligned} \quad (44)$$

and  $\Delta = \mu \sinh(\mu) - 2 \cosh(\mu) + 2$

As in the previous section, by considering the Taylor series expansion of these coefficients in terms of the tensile axial force parameter  $\mu$ , it can be shown that the first two terms exactly correspond to the classical coefficients given in Eq. (23).

### 3.4. The general stiffness matrix

The complete beam element is shown in Fig. 1(c) with two nodes and three degrees of freedom per node. This includes axial deformation in addition to the bending deformation discussed in the previous subsections. The displacements corresponding to degrees of freedom 1 and 4 relate to the axial deformation governed by Eq. (45), while the displacements corresponding to degrees of freedom 2, 3, 5 and 6 relate to the bending deformation governed by Eq. (16). When the axial deformation is considered, the governing equation is expressed by a second-order ordinary differential equation as

$$EA \frac{\partial^2 U(x)}{\partial x^2} = F_a(b) \quad (45)$$

where  $U(x)$  and  $F_a(x)$  are the axial displacement and applied axial forcing on the beam. Here  $EA$  is the axial stiffness of the beam and  $A$  is the area of the beam cross-section. The degrees of freedom in each node corresponds to the axial, transverse and rotational deformation. The stiffness matrix of the beam element in Fig. 1(c) can be expressed in the most general manner as

$$\mathbf{K}(\mu) = \begin{bmatrix} \frac{EA}{L} & 0 & 0 & -\frac{EA}{L} & 0 & 0 \\ 0 & \frac{d_1 EI}{L^3} & \frac{d_2 EI}{L^2} & 0 & -\frac{d_1 EI}{L^3} & \frac{d_2 EI}{L^2} \\ 0 & \frac{d_2 EI}{L^2} & \frac{d_3 EI}{L} & 0 & -\frac{d_2 EI}{L^2} & \frac{d_3 EI}{L} \\ -\frac{EA}{L} & 0 & 0 & \frac{EA}{L} & 0 & 0 \\ 0 & -\frac{d_1 EI}{L^3} & -\frac{d_2 EI}{L^2} & 0 & \frac{d_1 EI}{L^3} & -\frac{d_2 EI}{L^2} \\ 0 & \frac{d_2 EI}{L^2} & \frac{d_3 EI}{L} & 0 & -\frac{d_2 EI}{L^2} & \frac{d_3 EI}{L} \end{bmatrix} \quad (46)$$

The definition of the coefficients  $d_1 \cdots d_4$  will depend on whether compressive or tensile force is considered with the classical or exact beam theory as given by Eqs. (22), (23), (39) and (44).

We consider the beam to be of rectangular cross-section of thickness  $t$  and width  $b$ . The moment of inertia and the cross section area appearing in the stiffness matrix in Eq. (46) are given by

$$I = \frac{1}{12} bt^3 \quad (47)$$

$$\text{and } A = bt \quad (48)$$

To understand the error introduced from the use of the classical finite element stiffness matrix, we introduce a error measure. For a given stiffness coefficient,  $d_k, k = 1, \dots, 4$ , the error norm is defined as

$$\varepsilon_k = 100 \times \frac{d_{k\text{classical}} - d_k}{d_{k\text{EB}}}, \quad k = 1, 2, \dots, 4 \quad (49)$$

In the above equation,  $d_{k\text{EB}}$  are the stiffness coefficients from the conventional Euler-Bernoulli beam given in Eq. (24). In Fig. 3, this error is shown for the four unique coefficients for different values of the non-dimensional axial force  $\mu$ . Both cases, namely when the axial force is compressive and when the axial force is tensile are shown. Note the difference in the behaviour of the errors for the two case. The error is more when the force in compressive. We observe that for higher values of the compressive axial force, the error can go up to 10%. However, the error in the coefficient  $d_1$ , which is most important for the equivalent elastic properties, is generally less than 2%.

#### 4. Lattices under compressive stress

From the unit-cell derivations in Subsection 2.2, it can be observed that two coefficients of the  $6 \times 6$  element stiffness matrix of the inclined member and one coefficient of the  $6 \times 6$  element stiffness matrix of the vertical member, namely,  $K_{55}, K_{44}$  and  $K_{44}^{(h)}$ , are necessary to obtain  $E_1(\mu), E_2(\mu), \nu_{12}(\mu)$  and  $\nu_{21}(\mu)$ . The respective coefficients are given in the element stiffness matrix in Eq. (46). Using the expressions

of moment of inertia and the cross-sectional area in Eqs. (47) and (48), the stiffness coefficients are derived as

$$K_{55}(\mu) = \frac{d_1 EI}{L^3} = Eb\alpha^3 \frac{d_1}{12}, K_{44} = \frac{EA}{L} = Eb\alpha \quad \text{and} \quad K_{44}^{(h)} = \frac{EA}{h} = \frac{Ebt}{h} = \frac{Eb\alpha}{\beta} \quad (50)$$

Using these, we obtain the ratios

$$\frac{K_{55}(\mu)}{K_{44}} = \alpha^2 \frac{d_1}{12} \quad \text{and} \quad \frac{K_{55}(\mu)}{K_{44}^{(h)}} = \alpha^2 \beta \frac{d_1}{12} \quad (51)$$

Substituting these expressions in Eqs. (11)–(14) we obtain the general expressions

$$E_1(\mu) = \frac{E\alpha^3 \cos \theta}{(\beta + \sin \theta)(12 \sin^2 \theta / d_1 + \alpha^2 \cos^2 \theta)} \quad (52)$$

$$E_2(\mu) = \frac{E\alpha^3 (\beta + \sin \theta)}{(12/d_1 - \alpha^2) \cos^3 \theta + \alpha^2 (2\beta + 1) \cos \theta} \quad (53)$$

$$\nu_{12}(\mu) = \frac{\cos^2 \theta (12/d_1 - \alpha^2)}{(\beta + \sin \theta) \sin \theta (12/d_1 + \alpha^2 \cot^2 \theta)} \quad (54)$$

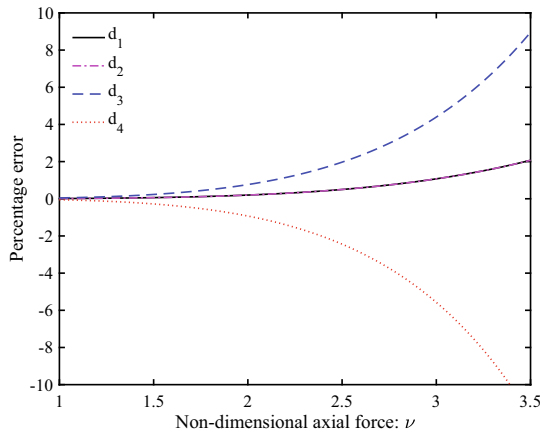
$$\nu_{21}(\mu) = \frac{(\beta + \sin \theta) \sin \theta (12/d_1 - \alpha^2)}{(12/d_1 - \alpha^2) \cos^3 \theta + \alpha^2 (2\beta + 1)} \quad (55)$$

For the shear modulus, five elements from two different stiffness matrices are necessary. They are two coefficients of the  $6 \times 6$  element stiffness matrix of the inclined member, namely,  $K_{65}, K_{44}$  and three elements of the stiffness matrix of the vertical member with half the length (see the supplementary document for further details). The vertical member is not subjected to any axial forcing due to the applied shear stress. Therefore, the only term in the expression of the shear modulus in Eq. (15) affected by axial stress is  $K_{65}$  corresponding to the inclined members of the unit cell. Therefore, we have

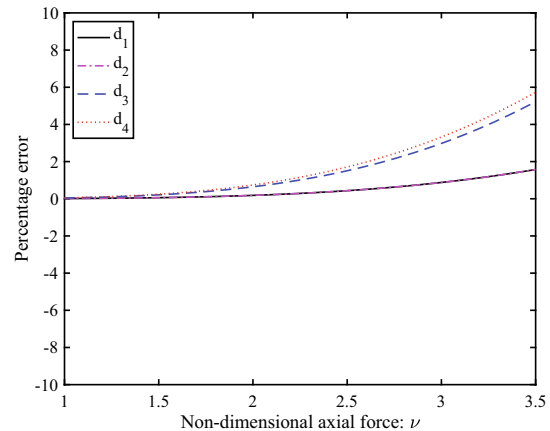
$$K_{65}(\mu) = -d_2 \frac{EI}{L^2} = -d_2 \frac{Ebt^3}{12L^2} \quad (56)$$

We also need three elements of the stiffness matrix of the vertical member with half the length given by

$$K_{55}^{(h/2)} = \frac{12EI}{(h/2)^3} = \frac{8Ebt^3}{h^3}, K_{56}^{(h/2)} = -\frac{6EI}{(h/2)^2} = -\frac{2Ebt^3}{h^2} \quad \text{and} \quad K_{66}^{(h/2)} = \frac{4EI}{(h/2)} = \frac{2Ebt^3}{3h} \quad (57)$$



(a) The axial force is compressive



(b) The axial force is tensile

Fig. 3. Errors in the four unique stiffness coefficients obtained using the classical approach in comparison with the exact transcendental stiffness coefficients as functions of the non-dimensional axial force  $\mu$ .

Using these expressions we obtain

$$G_{12}(\mu) = \frac{(\beta + \sin \theta)}{b \cos \theta} \frac{1}{\left( \frac{h^2}{2K_{65}(\mu)} + \frac{4k_{66}^{(h/2)}}{k_{55}^{(h/2)} k_{66}^{(h/2)} - (k_{56}^{(h/2)})^2 \right) + \frac{(\cos \theta + (\beta + \sin \theta) \tan \theta)^2}{K_{44}}} \quad (58)$$

$$= \frac{E\alpha^3(\beta + \sin \theta)}{(\beta^2(6/d_2 + 2\beta) + \alpha^2(\cos \theta + (\beta + \sin \theta) \tan \theta)^2) \cos \theta}$$

Substituting  $\alpha^2 = 0$  and taking the  $\lim_{\mu \rightarrow 0}$ , the equations derived here exactly reduce to the corresponding classical expressions by Gibson and Ashby [1] in Eqs. 4.5,7,8 (i.e., the case of considering only the bending deformation without any prestress). In this paper we are considering stresses in 1 and 2 directions only. Since this has limited effect on the shear modulus, in the following only  $E_1, E_2, \nu_{12}$  and  $\nu_{21}$  are discussed.

#### 4.1. Compressive stress in direction 1 only

In Fig. 4 we show the hexagonal lattice subjected to compressive stress in the 1-direction. In the same figure, forcing on the unit cell due this applied stress is also shown. It can be observed that the compressive axial force in the inclined beam is  $N = P \cos \theta$  where

$$P = \sigma_1 b(h + l \sin \theta) \quad (59)$$

Here  $\sigma_1$  is the applied stress and  $b$  is the out-of-plane thickness of the lattice. Using these, the non-dimensional axial force appearing in Eq. (20) can obtained as

$$\mu^2 = \frac{Nl^2}{EI} = \frac{\sigma_1 b(h + l \sin \theta) \cos \theta l^2}{Eb l^3 / 12} = \left( \frac{\sigma_1}{E} \right) \frac{12(\beta + \sin \theta) \cos \theta}{\alpha^3} \quad (60)$$

or  $\mu = \sqrt{\left( \frac{\sigma_1}{E\alpha^3} \right) 12(\beta + \sin \theta) \cos \theta}$

Using this expression of  $\mu$ , the non-dimensional coefficient  $d_1$  appearing in Eqs. (52)–(55) can be obtained either from Eq. (22) or Eq. (38) depending on whether the classical or the exact formulation is chosen. For the classical case, using  $d_1$  from Eq. (22) we have the approximate expressions

$$E_1^{(c)}(\mu) \approx \frac{E\alpha^3 \cos \theta}{(\beta + \sin \theta)(10 \sin^2 \theta / (10 - \mu^2) + \alpha^2 \cos^2 \theta)} \quad (61)$$

$$E_2^{(c)}(\mu) \approx \frac{E\alpha^3(\beta + \sin \theta)}{(10 / (10 - \mu^2) - \alpha^2) \cos^3 \theta + \alpha^2(2\beta + 1) \cos \theta} \quad (62)$$

$$\nu_{12}^{(c)}(\mu) \approx \frac{\cos^2 \theta (10 / (10 - \mu^2) - \alpha^2)}{(\beta + \sin \theta) \sin \theta (10 / (10 - \mu^2) + \alpha^2 \cot^2 \theta)} \quad (63)$$

$$\nu_{21}^{(c)}(\mu) \approx \frac{(\beta + \sin \theta) \sin \theta (10 / (10 - \mu^2) - \alpha^2)}{(10 / (10 - \mu^2) - \alpha^2) \cos^2 \theta + \alpha^2(2\beta + 1)} \quad (64)$$

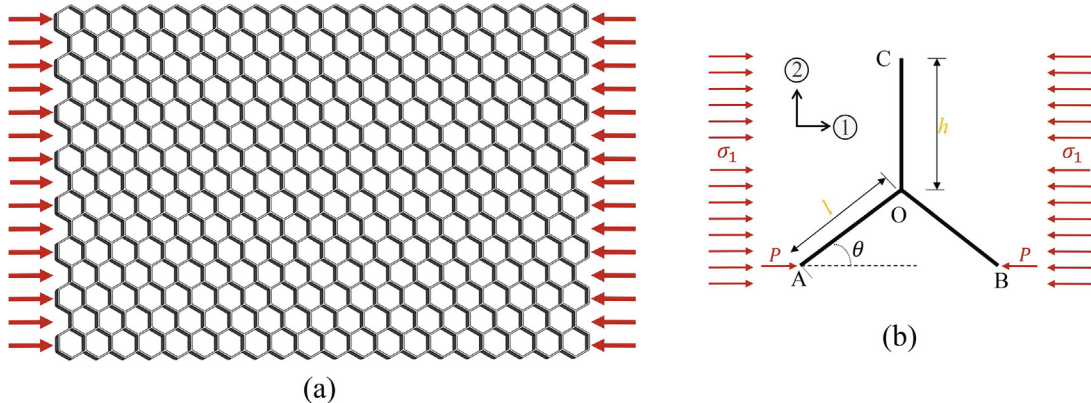


Fig. 4. (a) Hexagonal lattice subjected to compressive stress in the 1-direction. (b) Forcing in the constituent beams within the unit cell model. The compressive axial force is:  $P \cos \theta$  with  $P = \sigma_1 b(h + l \sin \theta)$ .

Here the superscript  $(\bullet)^{(c)}$  denotes that the elastic constants correspond to compressive stress in the lattice. It is evident from these expressions that all the four constants are nonlinear function of the stress parameter  $\mu$  explicitly obtained in (60).

The exact expression of the non-dimensional coefficient  $d_1$  is given in Eq. (38). Substituting this in Eqs. (52)–(55) and simplifying we obtain the exact expression of the elastic constants as

$$E_1^{(c)}(\mu) = \frac{E\alpha^3 \mu^3 \sin(\mu) \cos \theta}{(\beta + \sin \theta)(\mu^3 \sin(\mu) \alpha^2 \cos^2 \theta - 12 \sin^2 \theta \Delta)} \quad (65)$$

$$E_2^{(c)}(\mu) = \frac{E\alpha^3 \mu^3 \sin(\mu)(\beta + \sin \theta)}{\mu^3 \sin(\mu) \alpha^2 (2\beta + 1) \cos \theta - (\mu^3 \sin(\mu) \alpha^2 + 12\Delta) \cos^3 \theta} \quad (66)$$

$$\nu_{12}^{(c)}(\mu) = \frac{\cos^2 \theta (12\Delta + \mu^3 \sin(\mu) \alpha^2)}{(\beta + \sin \theta) \sin \theta (12\Delta - \mu^3 \sin(\mu) \alpha^2 \cot^2 \theta)} \quad (67)$$

$$\nu_{21}^{(c)}(\mu) = \frac{(\beta + \sin \theta) \sin \theta (12\Delta + \mu^3 \sin(\mu) \alpha^2)}{(12\Delta + \mu^3 \sin(\mu) \alpha^2) \cos^2 \theta - \mu^3 \sin(\mu) \alpha^2 (2\beta + 1)} \quad (68)$$

where  $\Delta = \mu \sin(\mu) - 2(1 - \cos(\mu))$ . As these expressions are in terms of trigonometric functions of the stress parameter  $\mu$  in Eq. (60), they represent a nonlinear relationship with the applied stress. A key difference between the approximate and exact expressions is that the approximate expressions in Eqs. (61)–(64) are in terms of  $\mu^2$ , while the exact expressions above are in terms of  $\sin(\mu)$ . Although the computational cost for both expressions are similar, the approximate expressions are simpler in nature. Only the exact expressions are used in this paper to demonstrate the numerical results. In the paragraph below, however, the results obtained from the exact and approximate expressions are compared.

In Fig. 5 analytical results are compared with direct nonlinear finite element simulation results. Equivalent normalised Young's modulus  $E_1/E\alpha^3$  is plotted as functions of the normalised compressive stress  $\sigma_1/E\alpha^3$  in direction 1 as shown in Fig. 4. The exact and approximate expressions given by Eq. (65) and Eq. (61) are also compared. Both expressions produce nearly identical results. In Fig. 5, the result obtained using the classical expression by Gibson and Ashby in Eq. (4) is also shown. The commercial software ANSYS has been used for the finite element results. Solid elements are used with 10 finite elements per beam has been employed for meshing. For the solution, the nonlinear analysis was used by invoking the 'large deformation' option. Although the results are not identical to the analytical expressions, the trend is similar and the error is within 10%. It is remarkable that even simple closed-form expressions such as the one in Eq. (61) produce an excellent agreement with the full scale nonlinear finite element analysis for the two different geometries analysed in Fig. 5. The two lattice

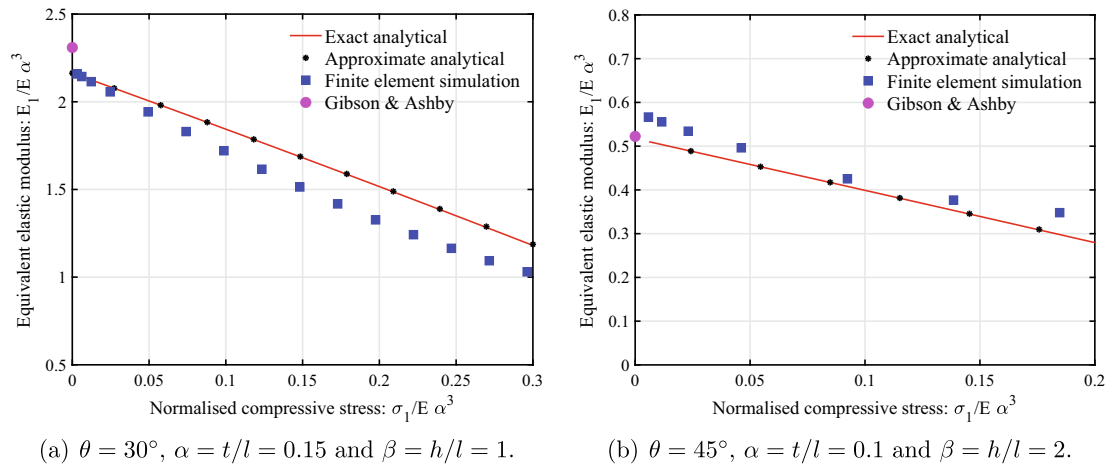


**Fig. 5.** Equivalent normalised Young’s modulus  $E_1/E\alpha^3$  plotted as functions of the normalised compressive stress  $\sigma_1/E\alpha^3$  in direction 1 as shown in Fig. 4. The results from analytical expressions are directly compared with the results from nonlinear finite element analysis. Two different lattice geometries are considered in (a) and (b).

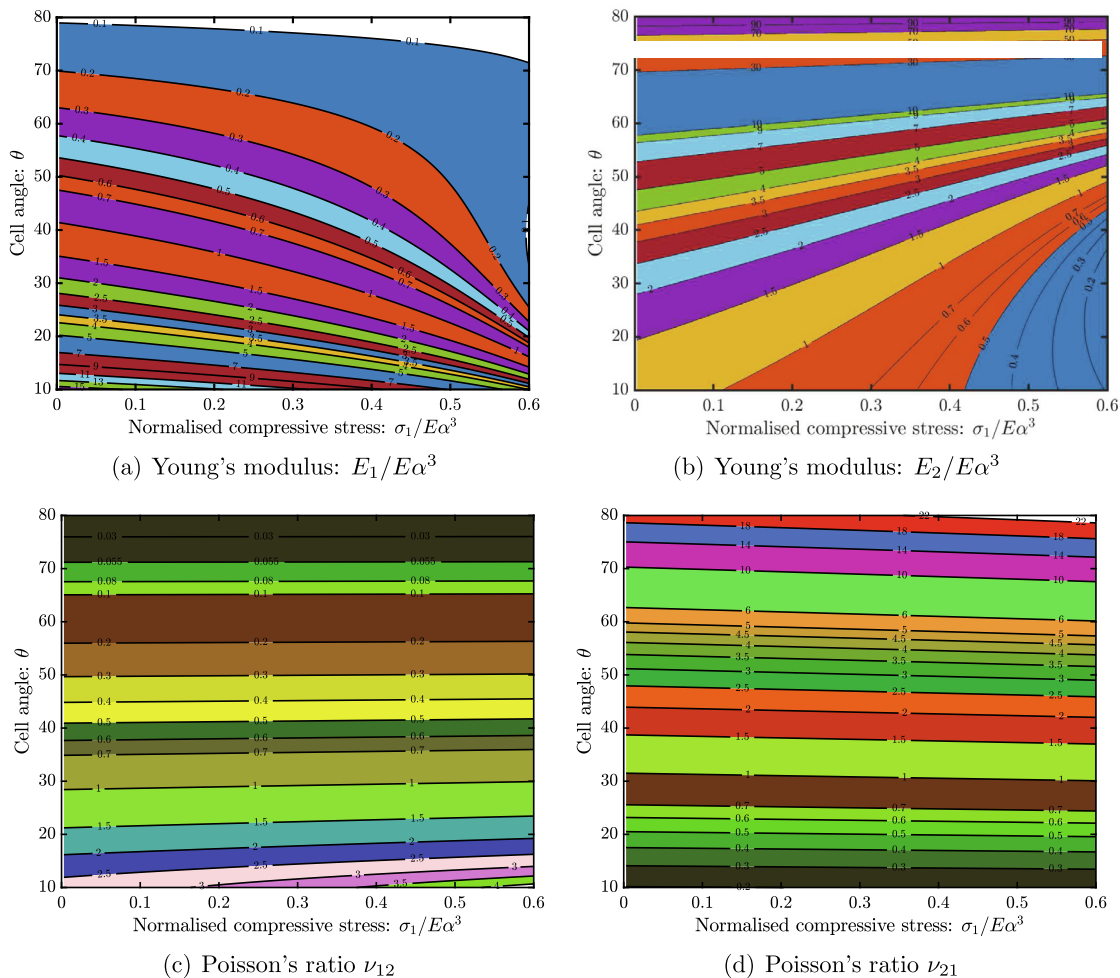


**Fig. 6.** Contours of the normalised effective elastic moduli and Poisson’s ratios of the lattice with compressive stress in direction 1 as depicted in Fig. 4. The normalised compressive stress  $\sigma_1/E\alpha^3$  is varied in the x-axis and the cell angle  $\theta$  is varied in the y-axis. The values of the geometric parameters used are  $\alpha = t/l = 0.15$  and  $\beta = h/l = 1$ .

geometries, namely,  $\theta = 30^\circ$ ,  $\alpha = 0.15$  and  $\beta = 1$  and  $\theta = 45^\circ$ ,  $\alpha = 0.1$  and  $\beta = 2$ , shown in Fig. 5 are for illustrative purposes only. The analytical formulation presented here is valid for the general case of 2D hexagonal lattices (see Subsection 6 later in the paper).

A key observation in Fig. 5 is that how the effective Young’s modulus becomes significantly lower from the classical result when the applied compressive stress is higher. To understand this further, in Fig. 6, contours of the normalised effective elastic moduli and



Poisson's ratios of the lattice with compressive stress in direction 1 are shown. Increasing cell angle has a decreasing effect on  $E_1$  and increasing effect on  $E_2$  for all values of the compressive stress. For the Poisson's ratios, increasing cell angle has a decreasing effect on  $\nu_{12}$  and increasing effect on  $\nu_{21}$  for all values of the compressive stress. Both the elastic moduli show a decreasing trend with the increasing compressive stress for all values of the cell angle  $\theta$ . This is to be expected as the lattice material loses stiffness due to the compressions (the stress softening effect in direction 1). The Poisson's ratios show a slightly increasing trend with increasing compressive stress.

#### 4.2. Compressive stress in direction 2 only

In Fig. 7 we show the hexagonal lattice subjected to compressive stress in the 2-direction. In the same figure, forcing on the unit cell due this applied stress is also shown. It can be observed that the compressive axial force in the inclined beam is  $N = W \sin \theta$  where

$$W = \sigma_2 b l \cos \theta \quad (69)$$

Here  $\sigma_2$  is the applied stress and  $b$  is the out-of-plane thickness of the lattice. Using these, the non-dimensional axial force appearing in Eq. (20) can be obtained as

$$\begin{aligned} \mu^2 &= \frac{Nl^2}{EI} = \frac{\sigma_2 b l \sin \theta \cos \theta l^2}{E b t^3 / 12} = \left(\frac{\sigma_2}{E}\right) \frac{12 \sin \theta \cos \theta}{\alpha^3} \\ \text{or } \mu &= \sqrt{\left(\frac{\sigma_2}{E \alpha^3}\right) 12 \sin \theta \cos \theta} \end{aligned} \quad (70)$$

The expressions of the equivalent elastic constants derived in Subsection 4.1 are valid with the expression of  $\mu$  given in Eq. (70). In Fig. 8 contours of the normalised effective elastic moduli and Poisson's ratios of the lattice with compressive stress in direction 2 are shown. Increasing cell angle has a decreasing effect on  $E_1$  and increasing effect on  $E_2$  for all values of the compressive stress. For the Poisson's ratios, increasing cell angle has a decreasing effect on  $\nu_{12}$  and increasing effect on  $\nu_{21}$  for all values of the compressive stress. Both the elastic moduli show a decreasing trend with the increasing compressive stress for all values of the cell angle  $\theta$ . Both the elastic moduli show a decreasing trend with the increasing compressive stress. This is to be expected as the lattice material loses stiffness due to the compressions

(the stress softening effect in direction 2). The Poisson's ratios do not show any significant change due to increasing compressive stress in the 2-direction.

#### 4.3. Compressive stresses in both directions

In Fig. 9 we show the hexagonal lattice subjected to compressive stresses applied simultaneously in both directions. In the same figure, forcing on the unit cell due these applied stresses are also shown. The fact that the axial force  $N$  within the individual beams are now functions of both  $\sigma_1$  and  $\sigma_2$ . From Fig. 9(b) we obtain the total axial forces as

$$N = P \cos \theta + W \sin \theta = \sigma_1 b (h + l \sin \theta) \cos \theta + \sigma_2 b l \sin \theta \cos \theta \quad (71)$$

The non-dimensional axial force parameter can be obtained as

$$\mu^2 = \frac{Nl^2}{EI} = \frac{\sigma_1 b (h + l \sin \theta) \cos \theta l^2 + \sigma_2 b l \sin \theta \cos \theta l^2}{E b t^3 / 12} \quad (72)$$

$$\text{or } \mu = \sqrt{12 \cos \theta \left\{ \left(\frac{\sigma_1}{E \alpha^3}\right) (\beta + \sin \theta) + \left(\frac{\sigma_2}{E \alpha^3}\right) \sin \theta \right\}} \quad (73)$$

The expressions of the equivalent elastic constants derived in Subsection 4.1 are valid with the expression of  $\mu$  given in Eq. (72). In Fig. 10 the effective elastic moduli and Poisson's ratio due to compressive stresses applied simultaneously in both directions are shown. The results are plotted as contour plots as functions of the normalised compressive stresses in both directions. Both Young's moduli are normalised by  $E \alpha^3$  and they show a decreasing trend with the increasing compressive stress values. This is to be expected as the lattice material loses stiffness due to the compressions. The Poisson's ratios do not show any significant change due to increasing compressive stress in both directions.

### 5. Lattices under tensile stress

In Section 4, exact closed-form expressions have been derived for  $E_1(\mu)$ ,  $E_2(\mu)$ ,  $\nu_{21}(\mu)$  and  $\nu_{12}(\mu)$  when the applied stress in both directions are compressive in nature. Eqs. (52)–(55) are general in nature and therefore also valid provided the stiffness coefficient  $d_1$  appearing in

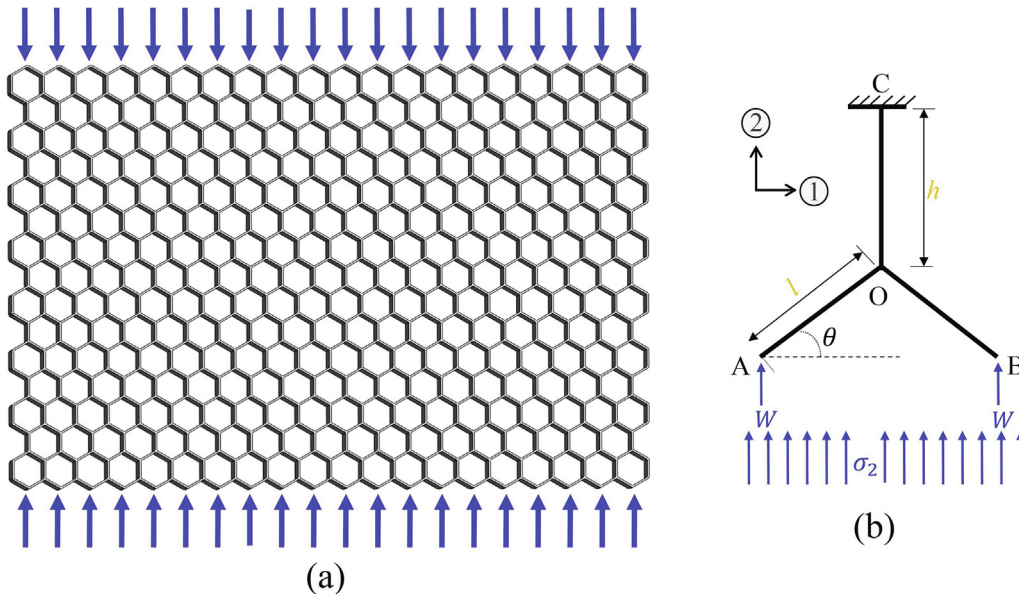
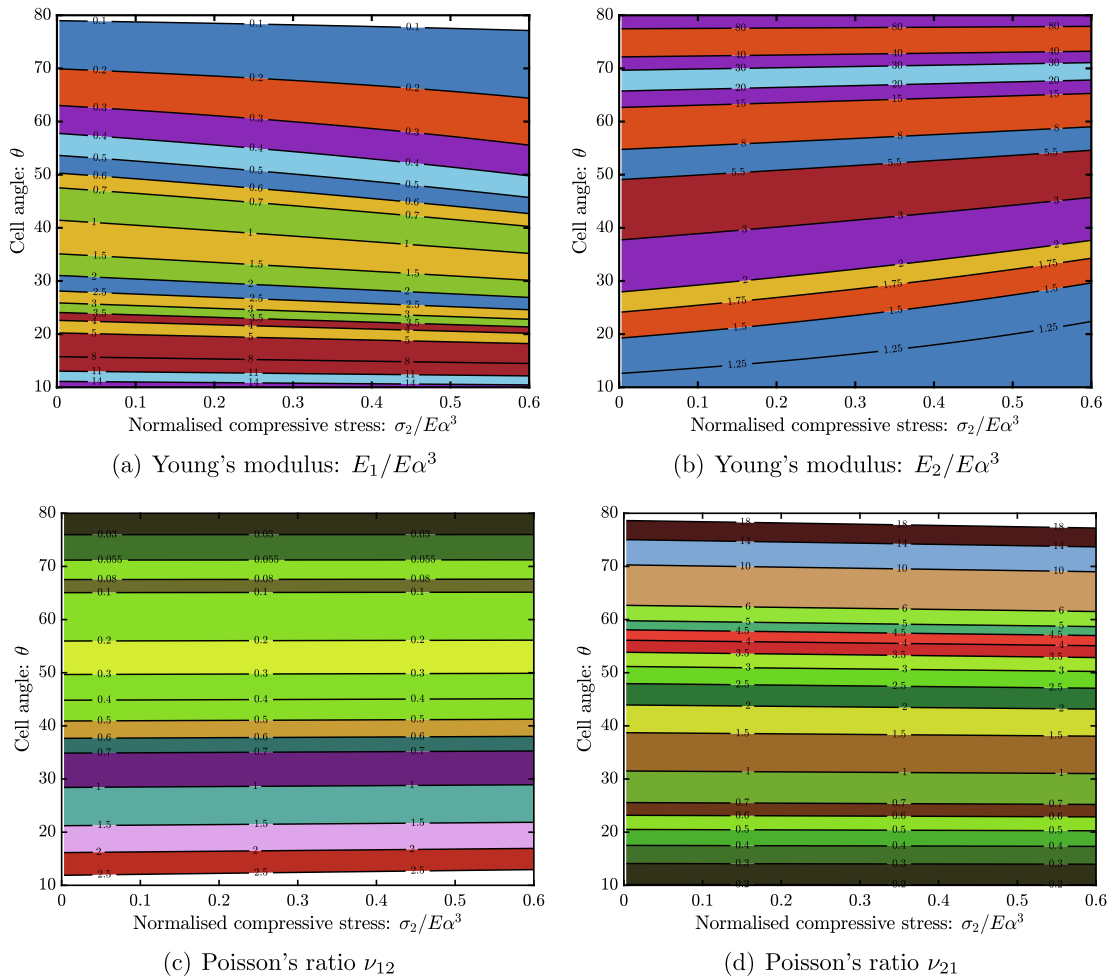
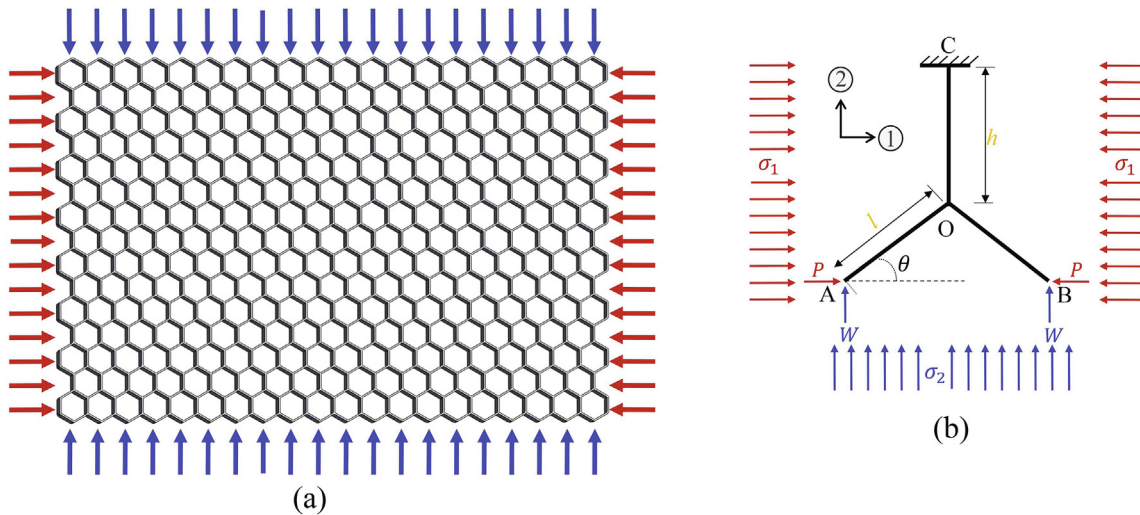


Fig. 7. (a) Hexagonal lattice subjected to compressive stress in the 2-direction. (b) Forcing in the constituent beams within the unit cell model. The compressive axial force is:  $W \sin \theta$  with  $W = \sigma_2 b l \cos \theta$ .



**Fig. 8.** Contours of the normalised effective elastic moduli and Poisson's ratios of the lattice with compressive stress in direction 2 as depicted in Fig. 7. The normalised compressive stress  $\sigma_2/E\alpha^3$  is varied in the  $x$ -axis and the cell angle  $\theta$  is varied in the  $y$ -axis. The values of the geometric parameters used are  $\alpha = t/l = 0.15$  and  $\beta = h/l = 1$ .



**Fig. 9.** (a) Hexagonal lattice subjected to compressive stress in both 1 and 2-directions. (b) Forcing in the constituent beams within the unit cell model. The compressive axial force is:  $P \cos \theta + W \sin \theta$  with  $P = \sigma_1 b(h + l \sin \theta)$  and  $W = \sigma_2 b l \cos \theta$ .

these equations are replaced by the case of tensile force in the beam. This can be obtained from Eq. (23) or (44) whether the classical

or the exact beam theory is employed. For the classical case, using  $d_1$  from Eq. (23) we have the approximate expressions

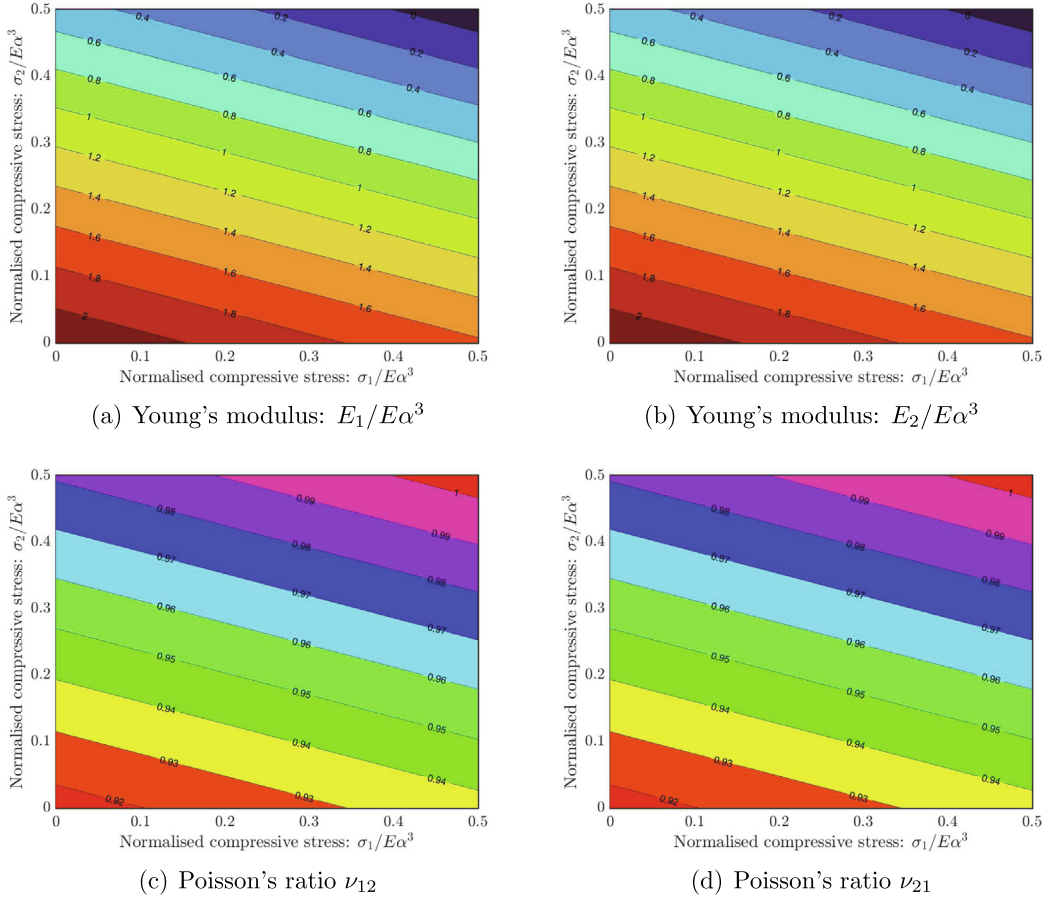


**Fig. 10.** The normalised effective elastic moduli and Poisson's ratios due to compressive stresses applied simultaneously in both directions. The contours are plotted as functions of the normalised compressive stresses in both directions with  $\alpha = t/l = 0.15$ ,  $\beta = h/l = 1$  and for a cell angle  $\theta = 30^\circ$ .

$$E_1^{(t)}(\mu) \approx \frac{E\alpha^3 \cos \theta}{(\beta + \sin \theta)(10 \sin^2 \theta / (10 + \mu^2) + \alpha^2 \cos^2 \theta)} \quad (74)$$

$$E_2^{(t)}(\mu) \approx \frac{E\alpha^3(\beta + \sin \theta)}{(10/(10 + \mu^2) - \alpha^2) \cos^2 \theta + \alpha^2(2\beta + 1) \cos \theta} \quad (75)$$

$$\nu_{12}^{(t)}(\mu) \approx \frac{\cos^2 \theta(12/d_1 - \alpha^2)}{(\beta + \sin \theta) \sin \theta(10/(10 + \mu^2) + \alpha^2 \cot^2 \theta)} \quad (76)$$

$$\nu_{21}^{(t)}(\mu) \approx \frac{(\beta + \sin \theta) \sin \theta(10/(10 + \mu^2) - \alpha^2)}{(10/(10 + \mu^2) - \alpha^2) \cos^2 \theta + \alpha^2(2\beta + 1)} \quad (77)$$

Here the superscript  $(\bullet)^{(t)}$  denotes that the elastic constants correspond to tensile stress in the lattice. It is evident from these expressions that all the four constants are a nonlinear function of the stress parameter  $\mu$ .

The exact expression of the non-dimensional coefficient  $d_1$  is given in Eq. (44). Substituting this in Eqs. (52)–(55) and simplifying we obtain the exact expression of the elastic constants as

$$E_1^{(t)}(\mu) = \frac{E\alpha^3 \mu^3 \sinh(\mu) \cos \theta}{(\beta + \sin \theta)(\mu^3 \sinh(\mu) \alpha^2 \cos^2 \theta + 12 \sin^2 \theta \Delta)} \quad (78)$$

$$E_2^{(t)}(\mu) = \frac{E\alpha^3 \mu^3 \sinh(\mu)(\beta + \sin \theta)}{\mu^3 \sinh(\mu) \alpha^2 (2\beta + 1) \cos \theta + (-\mu^3 \sinh(\mu) \alpha^2 + 12\Delta) \cos^3 \theta} \quad (79)$$

$$\nu_{12}^{(t)}(\mu) = \frac{\cos^2 \theta(12\Delta - \mu^3 \sinh(\mu) \alpha^2)}{(\beta + \sin \theta) \sin \theta(12\Delta + \mu^3 \sinh(\mu) \alpha^2 \cot^2 \theta)} \quad (80)$$

$$\nu_{21}^{(t)}(\mu) = \frac{(\beta + \sin \theta) \sin \theta(12\Delta - \mu^3 \sinh(\mu) \alpha^2)}{(12\Delta - \mu^3 \sinh(\mu) \alpha^2) \cos^2 \theta + \mu^3 \sinh(\mu) \alpha^2 (2\beta + 1)} \quad (81)$$

where  $\Delta = \mu \sinh(\mu) - 2 \cosh(\mu) + 2$ . As these expressions are in terms of hyperbolic functions of the stress parameter  $\mu$ , they represent a nonlinear relationship with the applied stress. Next we investigate the effect of tensile stress on the Elastic moduli and Poisson's ratios.

### 5.1. Tensile stress in direction 1 only

In Fig. 11 we show the hexagonal lattice subjected to tensile stress in the 1-direction. In the same figure, forcing on the unit cell due to this applied stress is also shown. The magnitude of the force is the same as in the case of equivalent compressive stress discussed in Subsection 4.1. Therefore the value of  $\mu$  is given by Eq. (60).

In Fig. 12 analytical results are compared with direct nonlinear finite element simulation results. Equivalent normalised Young's modulus  $E_1/E\alpha^3$  is plotted as functions of the normalised tensile stress  $\sigma_1/E\alpha^3$  in direction 1 as shown in Fig. 11. The exact and approximate expressions given by Eq. (78) and Eq. (74) are also compared. Both expressions produce nearly identical results. In Fig. 12, the result obtained using the classical expression by Gibson and Ashby in Eq. (4) is also shown. The commercial software ANSYS has been used for the finite element results. Solid elements are used with 10 finite elements per beam has been employed for meshing. For the solution, the nonlinear analysis was used by invoking the 'large deformation' option. The two lattice models considered here are the same as the

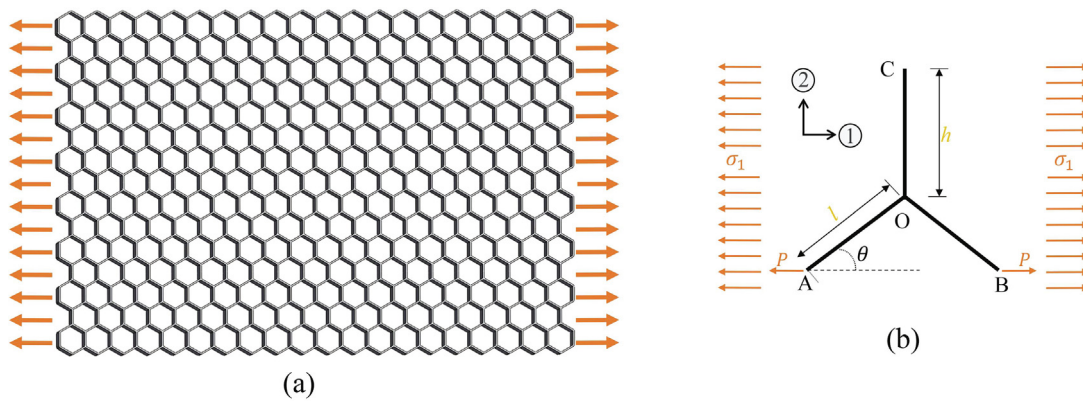


Fig. 11. (a) Hexagonal lattice subjected to tensile stress in the 1-direction. (b) Forcing in the constituent beams within the unit cell model. The tensile axial force is:  $P \cos \theta$  with  $P = \sigma_1 b(h + l \sin \theta)$ .

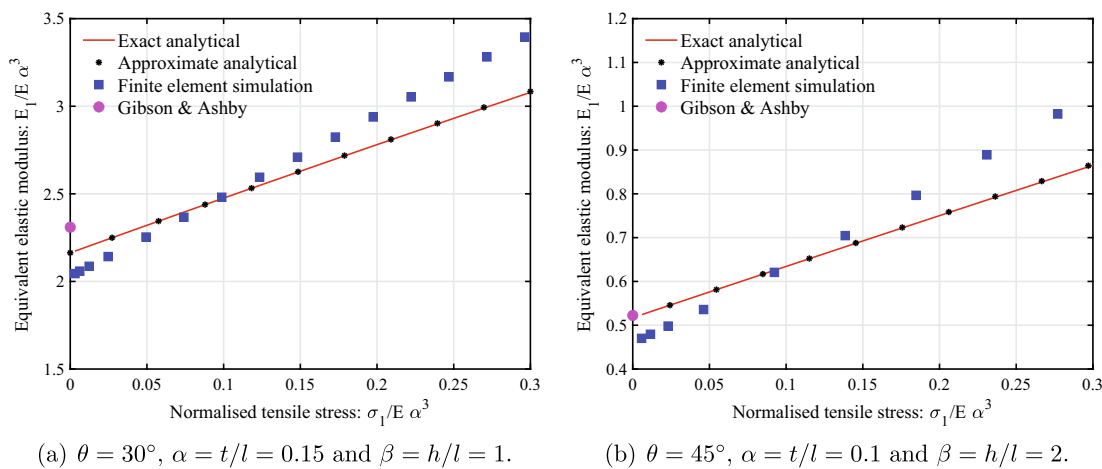


Fig. 12. Equivalent normalised Young's modulus  $E_1/Ea^3$  plotted as functions of the normalised tensile stress  $\sigma_1/Ea^3$  in direction 1 as shown in Fig. 11. The results from analytical expressions are directly compared with the results from nonlinear finite element analysis. Two different lattice geometries are considered in (a) and (b).

case of compressive stress discussed before. The direction of the stress has been reversed in the finite element analysis. Although the finite element results are not identical to the analytical expressions, the trend is similar and the error is within 10%. It is remarkable that even simple closed-form expressions such as the one in Eq. (74) produce an excellent agreement with the full scale nonlinear finite element analysis for the two different geometries analysed in Fig. 12.

A key observation in Fig. 12 is that how the effective Young's modulus is significantly higher from the classical result when the applied tensile stress is higher. To understand this further, in Fig. 13, contours of the normalised effective elastic moduli and Poisson's ratios of the lattice with tensile stress in direction 1 are shown. Increasing cell angle has a decreasing effect on  $E_1$  and increasing effect on  $E_2$  for all values of the tensile stress. For the Poisson's ratios, increasing cell angle has a decreasing effect on  $\nu_{12}$  and increasing effect on  $\nu_{21}$  for all values of the compressive stress. Both the elastic moduli show an increasing trend with the increasing tensile stress for all values of the cell angle  $\theta$ . This is to be expected as the lattice material becomes stiffer due to the tensile stress (the stress stiffening effect in direction 1). The Poisson's ratios show a slightly decreasing trend with the increasing tensile stress.

## 5.2. Tensile stress in direction 2 only

In Fig. 14 we show the hexagonal lattice subjected to tensile stress in the 2-direction. In the same figure, forcing on the unit cell due to

this applied stress is also shown. The magnitude of the force is the same as in the case of the equivalent compressive case discussed in Subsection 4.2. Therefore the value of  $\mu$  is given by Eq. (70).

In Fig. 15, contours of the normalised effective elastic moduli and Poisson's ratios of the lattice with tensile stress in direction 2 are shown. Increasing cell angle has a decreasing effect on  $E_1$  and increasing effect on  $E_2$  for all values of the tensile stress. For the Poisson's ratios, increasing cell angle has a decreasing effect on  $\nu_{12}$  and increasing effect on  $\nu_{21}$  for all values of the compressive stress. Both the elastic moduli show an increasing trend with the increasing tensile stress for all values of the cell angle  $\theta$ . This is to be expected as the lattice material becomes stiffer due to the tensile stress (the stress stiffening effect in direction 1). The Poisson's ratios do not show any significant change due to increasing tensile stress in the 2-direction.

## 5.3. Tensile stresses in both directions

In Fig. 16 we show the hexagonal lattice subjected to tensile stresses applied simultaneously in both directions. In the same figure, forcing on the unit cell due to these applied stresses are also shown. The magnitude of the force is the same as in the case of the equivalent compressive case discussed in Subsection 4.3. Therefore the value of  $\mu$  is given by Eq. (72).

In Fig. 17 the effective elastic moduli and Poisson's ratio due to tensile stresses applied simultaneously in both directions are shown. The

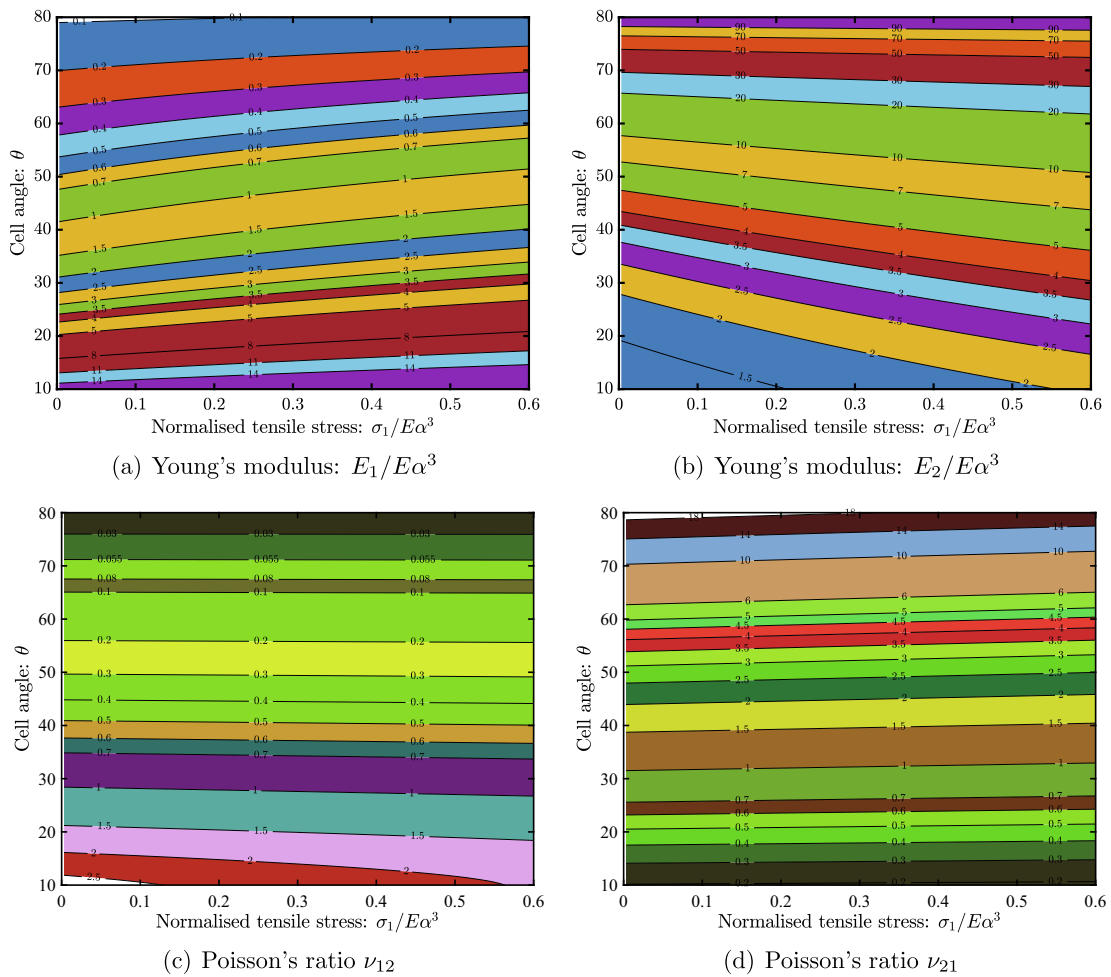


**Fig. 13.** Contours of the normalised effective elastic moduli and Poisson's ratios of the lattice with tensile stress in direction 1 as depicted in Fig. 11. The normalised tensile stress  $\sigma_1/E\alpha^3$  is varied in the x-axis and the cell angle  $\theta$  is varied in the y-axis. The values of the geometric parameters used are  $\alpha = t/l = 0.15$  and  $\beta = h/l = 1$ .

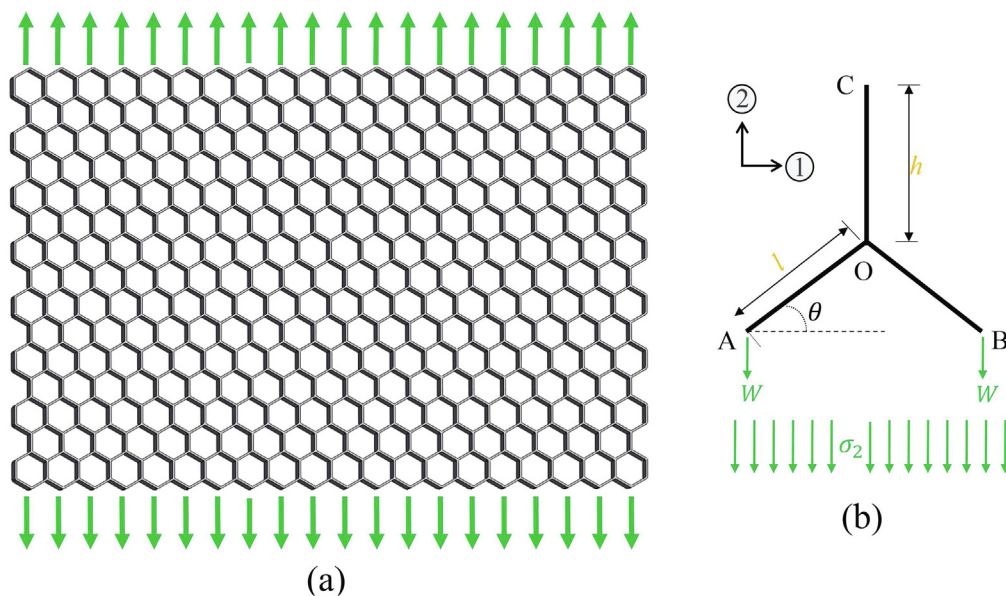


**Fig. 14.** (a) Hexagonal lattice subjected to tensile stress in the 2-direction. (b) Forcing in the constituent beams within the unit cell model. The tensile axial force is:  $W \sin \theta$  with  $W = \sigma_2 b l \cos \theta$ .

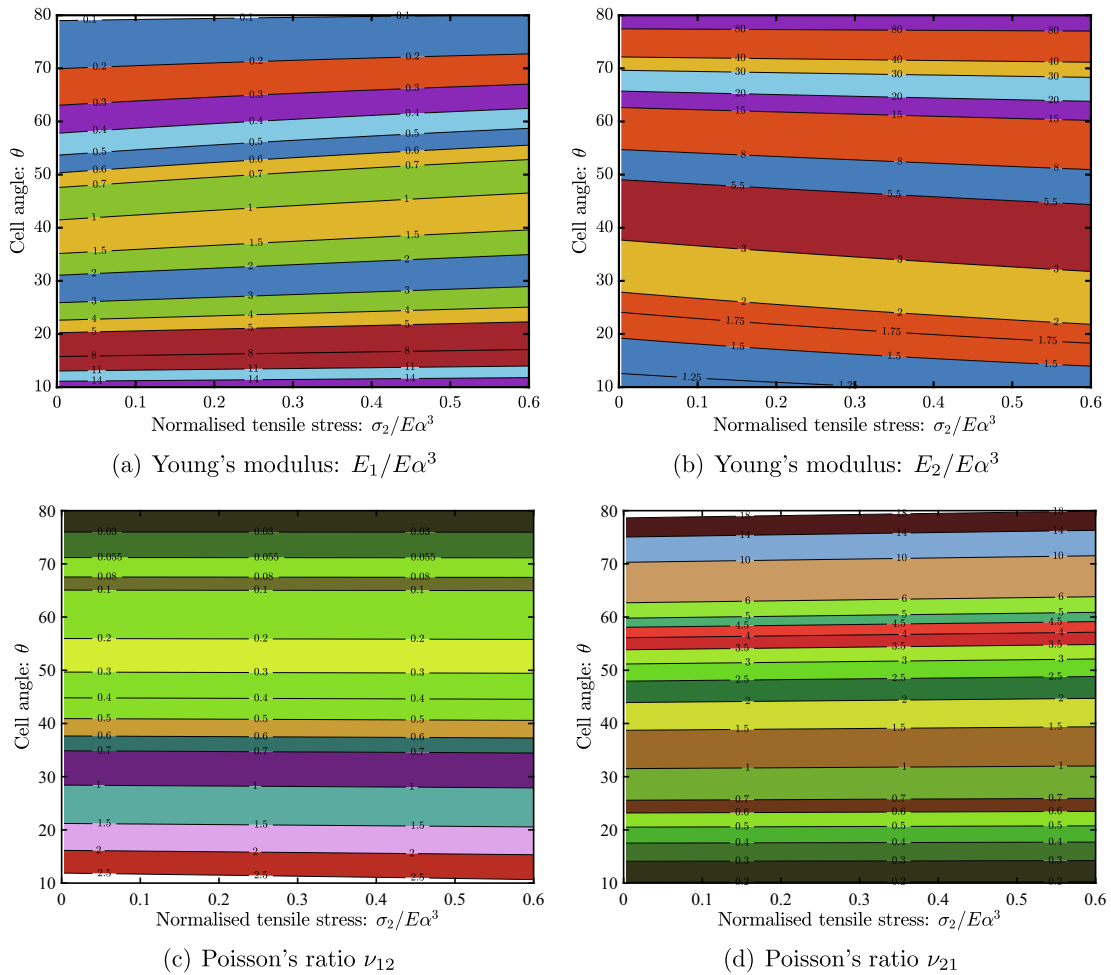


Fig. 15. Contours of the normalised effective elastic moduli and Poisson's ratios of the lattice with tensile stress in direction 2 as depicted in Fig. 14. The normalised tensile stress  $\sigma_2/E\alpha^3$  is varied in the x-axis and the cell angle  $\theta$  is varied in the y-axis. The values of the geometric parameters used are  $\alpha = t/l = 0.15$  and  $\beta = h/l = 1$ .

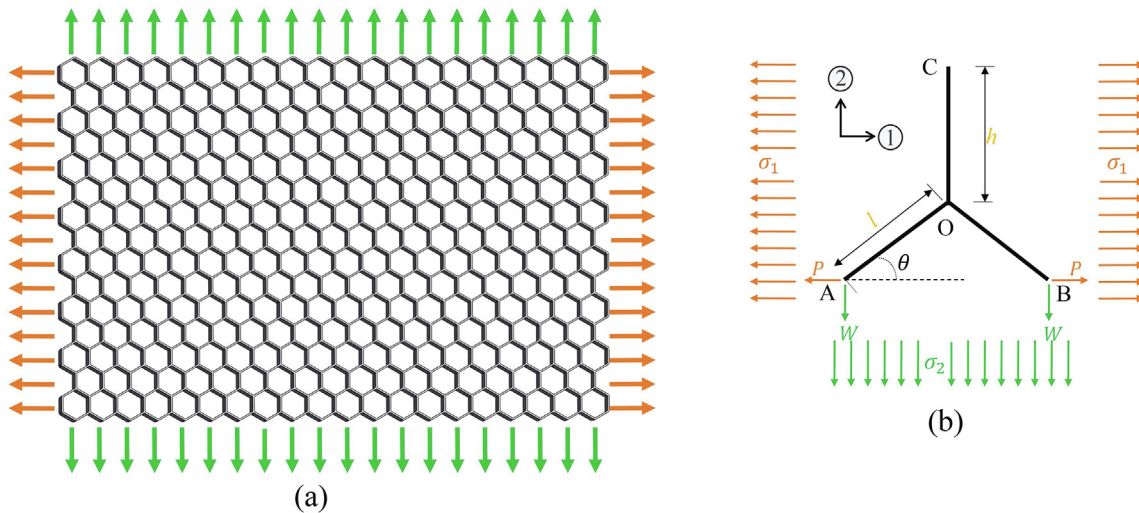
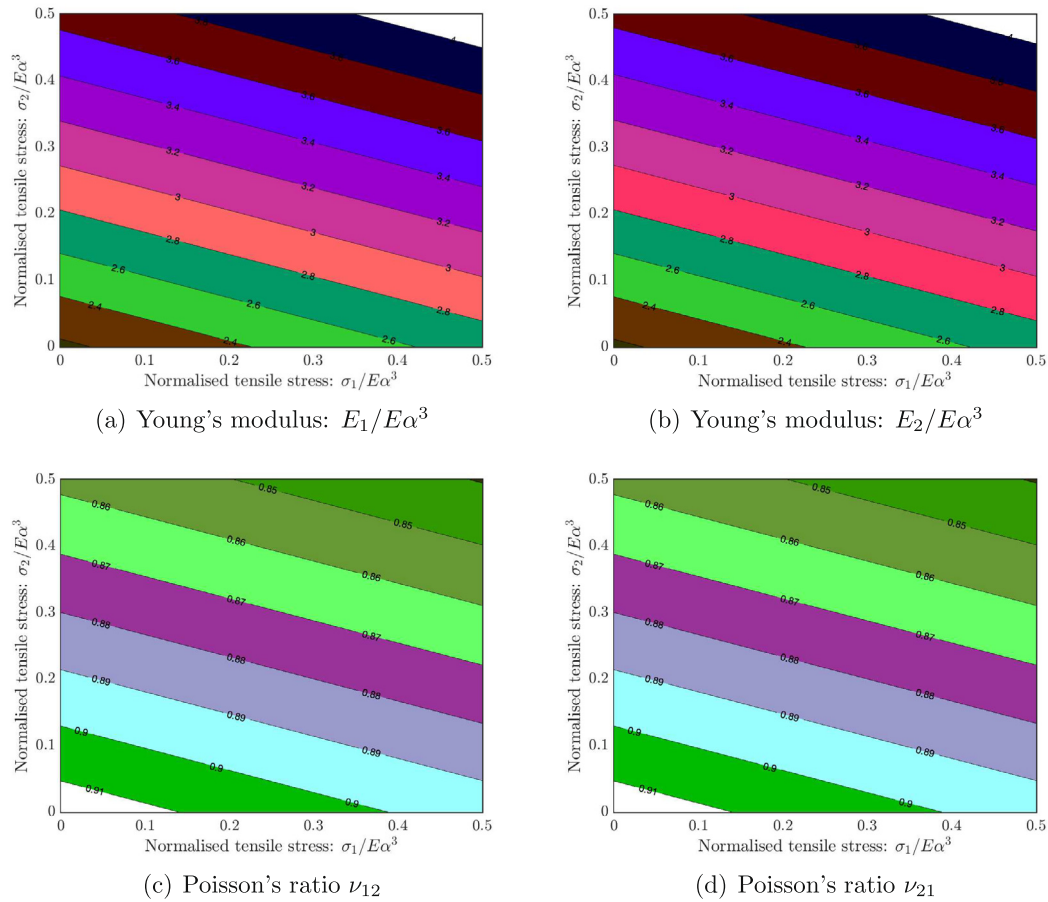


Fig. 16. (a) Hexagonal lattice subjected to tensile stress in both 1 and 2-directions. (b) Forcing in the constituent beams within the unit cell model. The tensile axial force is:  $P \cos \theta + W \sin \theta$  with  $P = \sigma_1 b (h + l \sin \theta)$  and  $W = \sigma_2 b l \cos \theta$ .

results are plotted as contour plots as functions of the normalised compressive stresses in both directions. Both Young's moduli are nor-

malised by  $E\alpha^3$  and they show an increasing trend with the increasing compressive stress values. This is consistent with the obser-



**Fig. 17.** The normalized effective elastic moduli and Poisson's ratios due to tensile stresses applied simultaneously in both directions. The contours are plotted as functions of the normalized tensile stresses in both direction with  $\alpha = t/l = 0.15, \beta = h/l = 1$  and for a cell angle  $\theta = 30^\circ$ .

vation in the previous two subsections. The Poisson's ratios do not show any significant change due to increasing compressive stress in both directions. They however remain less than 1 for the parameter range selected here.

**6. The analysis of different lattice geometries**

The general formulation developed here allows the proposed analytical framework to be applied to various other lattice patterns and geometry of the constituent members. Three special cases of wide

interest are shown in Fig. 18. They include the auxetic lattice ( $\theta$  is negative), the rhombus lattice ( $h = 0$ ) and the rectangular lattice ( $\theta = 0$ ). The degenerated unit cells are highlighted in the figure. Next, we explicitly derive the equivalent elastic moduli and Poisson's ratios for these three special cases.

**6.1. The auxetic lattice:  $\theta$  is negative**

The auxetic or re-entrant lattice is obtained when the angle  $\theta$  is negative. The unit cell and the corresponding lattice material is shown

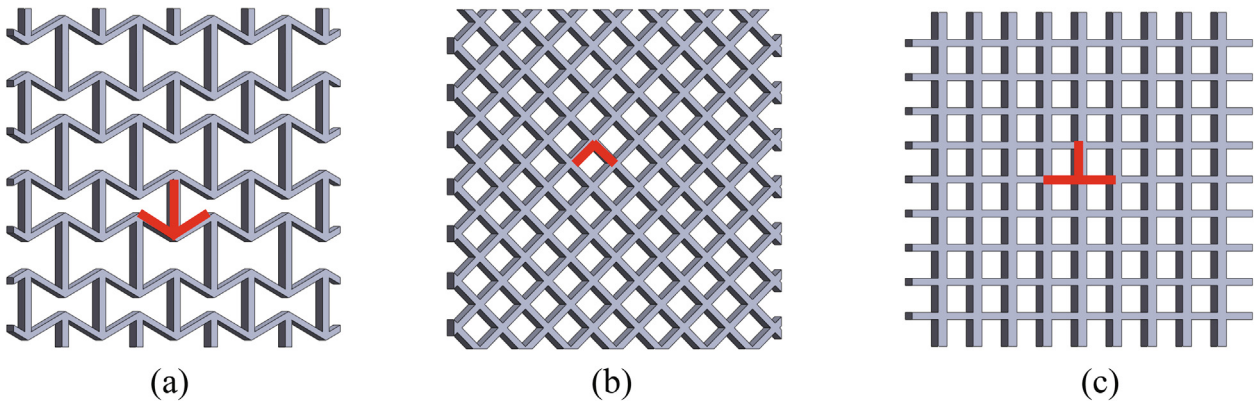


**Fig. 18.** Three distinct types of 2D lattices arising due to special geometric cases. (a) The auxetic lattice:  $\theta$  is negative, (b) The rhombus lattice:  $h = 0$  and (c) The rectangular lattice:  $\theta = 0$ . The degenerated unit cells are highlighted in the figures.

in Fig. 18(a). Therefore, taking the case  $\theta = -\theta$  in Eqs. (60) and (70), the axial force parameter for the two directions can be obtained as

$$\text{For direction 1 : } \mu^2 = \left(\frac{\sigma_1}{E\alpha^3}\right) 12(\beta - \sin \theta) \cos \theta \quad (82)$$

and

$$\text{For direction 2 : } \mu^2 = -\left(\frac{\sigma_2}{E\alpha^3}\right) 12 \sin \theta \cos \theta \quad (83)$$

It is important to observe that  $\mu^2$  is negative for the stress in 2-direction. This can be physically verified from the unit cell configuration in Fig. 18(a). Therefore, when the stress in direction 2 is considered, the value of  $d_1$  and  $d_2$  must be altered from that in direction 1. For a compressive  $\sigma_2$  one need to use the stiffness coefficients for the tensile case in Eq. (44), and for a tensile  $\sigma_2$  one need to use the stiffness coefficients for the compressive case in Eq. (38). Once the axial force parameter  $\mu$  is obtained, the equivalent elastic properties of the auxetic lattice can be derived from Eqs. (52)–(55) by substituting  $\theta = -\theta$  as

$$E_1(\mu) = \frac{E\alpha^3 \cos \theta}{(\beta - \sin \theta)(12 \sin^2 \theta/d_1 + \alpha^2 \cos^2 \theta)} \quad (84)$$

$$E_2(\mu) = \frac{E\alpha^3(\beta - \sin \theta)}{(12/d_1 - \alpha^2) \cos^3 \theta + \alpha^2(2\beta + 1) \cos \theta} \quad (85)$$

$$\nu_{12}(\mu) = -\frac{\cos^2 \theta(12/d_1 - \alpha^2)}{(\beta - \sin \theta) \sin \theta(12/d_1 + \alpha^2 \cot^2 \theta)} \quad (86)$$

$$\nu_{21}(\mu) = -\frac{(\beta - \sin \theta) \sin \theta(12/d_1 - \alpha^2)}{(12/d_1 - \alpha^2) \cos^2 \theta + \alpha^2(2\beta + 1)} \quad (87)$$

The shear modulus can also be obtained from (58) as

$$G_{12}(\mu) = \frac{E\alpha^3(\beta - \sin \theta)}{(\beta^2(6/d_2 + 2\beta) + \alpha^2(\cos \theta - (\beta - \sin \theta) \tan \theta)^2) \cos \theta} \quad (88)$$

### 6.2. The rhombus lattice: $h = 0$

The rhombus lattice is obtained when  $h = \beta = 0$ . This implies the absence of the vertical member in the unit cell as shown in Fig. 1. The revised unit cell and the corresponding lattice material is shown in Fig. 18(b). Taking the limit  $\beta = 0$  in Eq. (60), the axial force parameter for stress in direction 1 can be obtained as

$$\mu = \lim_{\beta \rightarrow 0} \sqrt{\left(\frac{\sigma_1}{E\alpha^3}\right) 12(\beta + \sin \theta) \cos \theta} = \sqrt{\left(\frac{\sigma_1}{E\alpha^3}\right) 12 \sin \theta \cos \theta} \quad (89)$$

The axial force parameter for stress in direction 2 is unaltered and given by Eq. (70) as this is not a function of  $\beta$ . Once the axial force parameter  $\mu$  is obtained, the equivalent elastic properties of the rhombus lattice can be derived from Eqs. (52)–(55) by taking the limit  $\beta = 0$  as

$$E_1(\mu) = \lim_{\beta \rightarrow 0} \frac{E\alpha^3 \cos \theta}{(\beta + \sin \theta)(12 \sin^2 \theta/d_1 + \alpha^2 \cos^2 \theta)} = \frac{E\alpha^3 \cos \theta}{\sin \theta(12 \sin^2 \theta/d_1 + \alpha^2 \cos^2 \theta)} \quad (90)$$

$$E_2(\mu) = \lim_{\beta \rightarrow 0} \frac{E\alpha^3(\beta + \sin \theta)}{(12/d_1 - \alpha^2) \cos^3 \theta + \alpha^2(2\beta + 1) \cos \theta} = \frac{E\alpha^3 \sin \theta}{\cos \theta(12 \cos^2 \theta/d_1 + \alpha^2 \sin^2 \theta)} \quad (91)$$

$$\nu_{12}(\mu) = \lim_{\beta \rightarrow 0} \frac{\cos^2 \theta(12/d_1 - \alpha^2)}{(\beta + \sin \theta) \sin \theta(12/d_1 + \alpha^2 \cot^2 \theta)} = \frac{\cos^2 \theta(12/d_1 - \alpha^2)}{12 \sin^2 \theta/d_1 + \alpha^2 \cos^2 \theta} \quad (92)$$

$$\begin{aligned} \nu_{21}(\mu) &= \lim_{\beta \rightarrow 0} \frac{(\beta + \sin \theta) \sin \theta(12/d_1 - \alpha^2)}{(12/d_1 - \alpha^2) \cos^2 \theta + \alpha^2(2\beta + 1)} \\ &= \frac{\sin^2 \theta(12/d_1 - \alpha^2)}{(12 \cos^2 \theta/d_1 + \alpha^2 \sin^2 \theta)} \end{aligned} \quad (93)$$

The shear modulus can be obtained in a similar manner from Eq. (58) as

$$G_{12}(\mu) = \lim_{\beta \rightarrow 0} \frac{E\alpha^3(\beta + \sin \theta)}{(\beta^2(6/d_2 + 2\beta) + \alpha^2(\cos \theta + (\beta + \sin \theta) \tan \theta)^2) \cos \theta} = E\alpha \sin \theta \cos \theta \quad (94)$$

### 6.3. The rectangular lattice: $\theta = 0$

The rectangular lattice is obtained when  $\theta = 0$ . This implies that the two inclined beams become aligned in the unit cell shown in Fig. 1. The revised unit cell and the corresponding lattice material is shown in Fig. 18(c). Taking the limit  $\theta = 0$  in Eq. (60), the axial force parameter for stress in direction 1 can be obtained as

$$\mu = \lim_{\theta \rightarrow 0} \sqrt{\left(\frac{\sigma_1}{E\alpha^3}\right) 12(\beta + \sin \theta) \cos \theta} = \sqrt{\left(\frac{\sigma_1}{E\alpha^3}\right) 12\beta} \quad (95)$$

The axial force parameter for stress in direction 2 given by Eq. (70) becomes 0 when  $\theta = 0$ . This implies that the stress in direction 2 does not have any effect on the elastic properties of a rectangular lattice. The equivalent elastic properties of the rhombus lattice can be derived from Eqs. (52)–(55) by taking the limit  $\theta = 0$  as

$$E_1(\mu) = \lim_{\theta \rightarrow 0} \frac{E\alpha^3 \cos \theta}{(\beta + \sin \theta)(12 \sin^2 \theta/d_1 + \alpha^2 \cos^2 \theta)} = \frac{E\alpha}{\beta} \quad (96)$$

$$E_2(\mu) = \lim_{\theta \rightarrow 0} \frac{E\alpha^3(\beta + \sin \theta)}{(12/d_1 - \alpha^2) \cos^3 \theta + \alpha^2(2\beta + 1) \cos \theta} = \frac{E\alpha^3 \beta}{12/d_1 + 2\alpha^2 \beta} \quad (97)$$

$$\nu_{12}(\mu) = \lim_{\theta \rightarrow 0} \frac{\cos^2 \theta(12/d_1 - \alpha^2)}{(\beta + \sin \theta) \sin \theta(12/d_1 + \alpha^2 \cot^2 \theta)} = 0 \quad (98)$$

$$\nu_{21}(\mu) = \lim_{\theta \rightarrow 0} \frac{(\beta + \sin \theta) \sin \theta(12/d_1 - \alpha^2)}{(12/d_1 - \alpha^2) \cos^2 \theta + \alpha^2(2\beta + 1)} = 0 \quad (99)$$

We observe that  $E_1$  is independent of the applied stress and both the Poisson's ratios are zero. The shear modulus can be obtained in a similar manner from Eq. (58) as

$$G_{12}(\mu) = \lim_{\theta \rightarrow 0} \frac{E\alpha^3(\beta + \sin \theta)}{(\beta^2(6/d_2 + 2\beta) + \alpha^2(\cos \theta + (\beta + \sin \theta) \tan \theta)^2) \cos \theta} = \frac{E\alpha^3 \beta}{\beta^2(6/d_2 + 2\beta) + \alpha^2} \quad (100)$$

## 7. Conclusions

The in-plane mechanics of highly stretchable and compressible lattice materials is considered. A key feature of this problem in the underlying geometric nonlinearly leading to axial softening and stiffening of the constituent beam elements. A physics-based analytical approach leading to closed-form expressions of in-plane equivalent elastic properties of hexagonal lattices was presented. The route to this analytical derivation has three key steps. Firstly, noting that the constitutive members of lattices are thin beams, stiffness matrices of beams under compression and tension are derived exactly. This is achieved using transcendental displacement functions which are exact solutions of the governing ordinary differential equation with appropriate boundary conditions. Secondly, using the mechanics of a selected unit cell, Young's moduli, Poisson's ratios and the shear modulus of the lattice were derived such that the resulting expressions utilise the stiffness matrix derived in the first step. Finally, combining these two steps,



equivalent elastic properties were obtained for compressed and stretched lattices. Equivalent elastic properties are nonlinear functions of applied compressive stresses (through trigonometric functions) and tensile stresses (through hyperbolic functions). This results in a nonlinear homogeneous stress-strain relationship for the cellular material. Key novel features of this paper include:

- A general methodology for deriving equivalent elastic properties of hexagonal lattices using the coefficients of the stiffness matrix of the constituent beams.
- The explicit employment of ordinary differential equations governing the deformation of axially loaded beams and incorporating the results into the unit cell based analysis.
- The direct quantification of the impact of external compressive and tensile stresses on the equivalent elastic properties through exact closed-form expressions.
- The generalised nature of the newly derived expressions arising from the fact that many special cases of interest are identified by taking approximate mathematical limits.

It was shown that the general expressions of the equivalent elastic properties can be used to investigate three special cases of wide interest, namely, auxetic hexagonal lattices, rhombus-shaped lattices and rectangular lattices.

The analytical expressions have been validated with the results from commercial finite element software with nonlinear analysis for both compressive and tensile stresses. Results obtained from the expressions derived are graphically illustrated as functions of applied compressive and tensile stresses. Three scenarios are considered for each case, namely, when the stress is applied in directions 1 and 2 separately and together. For the case of compressive stress, a decrease in the effective elastic moduli was observed. On the contrary, for the case of tensile stress, an increase in the effective elastic moduli was observed. The effect of external stresses on both the Poisson's ratios was insignificant. The closed-form expressions derived here to provide excellent opportunities to use them for design and optimisation of highly stretchable and compressible 2D lattices in a computationally efficient and physically appealing manner. Application domains of this work will include industrial sectors which exploit highly compressible and stretchable lattice materials. Specific examples include, but are not limited to, energy absorbent foams, elastomers, soft robotics, next-generation stent technology, stain-based biosensors, foldable and adaptive lattices, flexible mechanical and acoustic metamaterials. Although geometric nonlinearity arising due to large deformation is included in this work, the material behaviours are assumed to be linear. Future works in this direction should focus on nonlinear material behaviour to encompass a wide range of materials available to manufacture lattice materials.

#### Declaration of Competing Interest

The authors declare that they have no known competing financial interests or personal relationships that could have appeared to influence the work reported in this paper.

#### Acknowledgements

The author gratefully acknowledges the financial support from H2020 Marie Skłodowska-Curie Actions project METASINK, Grant No.: MSCA-IF-2019-896942. Help from Ms. M. F. Arago towards the finite element results and illustrative diagrams appearing in this paper is highly acknowledged.

#### Appendix A. Supplementary data

Supplementary data associated with this article can be found, in the online version, at <https://doi.org/10.1016/j.compstruct.2021.114167>.

#### References

- [1] Gibson L, Ashby MF. Cellular solids structure and properties. Cambridge, UK: Cambridge University Press; 1999.
- [2] Fleck NA, Deshpande VS, Ashby MF, past Micro-architected materials: present and future. Proc R Soc London A 2010;466(2121):2495–516.
- [3] Scarpa F, Adhikari S, Gil AJ, Remillat C. The bending of single layer graphene sheets: lattice versus continuum approach. Nanotechnology 2010;20(12):085405.
- [4] Chandra Y, Chowdhury R, Adhikari S, Scarpa F. Elastic instability of bilayer graphene using atomistic finite element. Physica E 2011;44(1):12–6.
- [5] Boldrin L, Scarpa F, Chowdhury R, Adhikari S, Ruzzene M. Effective mechanical properties of hexagonal boron nitride nanosheets. Nanotechnology 2011;22(50):505702:1–7.
- [6] Mukhopadhyay T, Mahata T, Adhikari S, Zaeem MA. Effective mechanical properties of multilayer nano-heterostructures. Nat Scientific Rep 2017;7(1):15818:1–13.
- [7] Amendola A, Smith C, Goodall R, Auricchio F, Feo L, Benzoni G, Fraternali F. Experimental response of additively manufactured metallic pentamode materials confined between stiffening plates. Compos Struct 2016;142:254–62.
- [8] Amendola A, Carpentieri G, Feo L, Fraternali F. Bending dominated response of layered mechanical metamaterials alternating pentamode lattices and confinement plates. Compos Struct 2016;157:71–7.
- [9] El-Sayed FKA, Jones R, Burgess IW. A theoretical approach to the deformation of honeycomb based composite materials. Composites 1979;10(4):209–14.
- [10] Zhang J, Ashby MF. The out-of-plane properties of honeycombs. Int J Mech Sci 1992;34(6):475–89.
- [11] Malek S, Gibson L. Effective elastic properties of periodic hexagonal honeycombs. Mech Mater 2015;91:226–40.
- [12] Huang T, Gong Y, Zhao S. Effective in-plane elastic modulus of a periodic regular hexagonal honeycomb core with thick walls. J Eng Mech 2018;144(2):06017019.
- [13] Balawi S, Abot J. The effect of honeycomb relative density on its effective in-plane elastic moduli: An experimental study. Compos Struct 2008;84(4):293–9.
- [14] Tauhiduzzaman M, Carlsson LA. Influence of constraints on the effective inplane extensional properties of honeycomb core. Compos Struct 2019;209:616–24.
- [15] Adhikari S, Mukhopadhyay T, Liu X. Broadband dynamic elastic moduli of honeycomb lattice materials: A generalized analytical approach. Mech Mater 2021;157(6):103796.
- [16] Ongaro F. Estimation of the effective properties of two-dimensional cellular materials: a review. Theor Appl Mech Lett 2018;8(4):209–30.
- [17] Mukhopadhyay T, Adhikari S. Effective in-plane elastic properties of quasi-random spatially irregular hexagonal lattices. Int J Eng Sci 2017;119(10):142–79.
- [18] Papka SD, Kyriakides S. In-plane compressive response and crushing of honeycomb. J Mech Phys Solids 1994;42(10):1499–532.
- [19] Triantafyllidis N, Schraad MW. Onset of failure in aluminum honeycombs under general in-plane loading. J Mech Phys Solids 1998;46(6):1089–124.
- [20] Klintworth J, Stronge W. Elasto-plastic yield limits and deformation laws for transversely crushed honeycombs. Int J Mech Sci 1988;30(3–4):273–92.
- [21] Cote F, Deshpande V, Fleck N, Evans A. The out-of-plane compressive behavior of metallic honeycombs. Mater Sci Eng: A 2004;380(1–2):272–80.
- [22] Li K, Gao XL, Wang J. Dynamic crushing behavior of honeycomb structures with irregular cell shapes and non-uniform cell wall thickness. Int J Solids Struct 2007;44(14–15):5003–26.
- [23] Liu W, Wang N, Huang J, Zhong H. The effect of irregularity, residual convex units and stresses on the effective mechanical properties of 2d auxetic cellular structure. Mater Sci Eng: A 2014;609:26–33.
- [24] Ruan D, Lu G, Wang B, Yu T. In-plane dynamic crushing of honeycombs finite element study. Int J Impact Eng 2003;28(2):161–82.
- [25] Zheng Z, Yu J, Li J. Dynamic crushing of 2d cellular structures: a finite element study. Int J Impact Eng 2005;32(1–4):650–64.
- [26] Yue X-Z, Matsuo K, Kitazono K. Compressive behavior of open-cell titanium foams with different unit cell geometries. Mater Trans 2017;58(11):1587–92.
- [27] Zhang M, Yang Z, Lu Z, Liao B, He X. Effective elastic properties and initial yield surfaces of two 3d lattice structures. Int J Mech Sci 2018;138:146–58.
- [28] Amendola A, Fraternali F. Incremental auxetic response of composite lattices under isotropic prestress. Compos Struct 2018;191:145–53.
- [29] Tan H, He Z, Li K, Li E, Cheng A, Xu B. In-plane crashworthiness of re-entrant hierarchical honeycombs with negative poisons ratio. Compos Struct 2019;229:111415.
- [30] Yang X, Xi X, Pan Q, Liu H. In-plane dynamic crushing of a novel circular-celled honeycomb nested with petal-shaped mesostructure. Compos Struct 2019;226:111219.
- [31] Sorohan S, Constantinescu DM, Sandu M, Sandu AG. On the homogenization of hexagonal honeycombs under axial and shear loading, part i: analytical formulation for free skin effect. Mech Mater 2018;119:74–91.
- [32] Sorohan S, Constantinescu DM, Sandu M, Sandu AG. On the homogenization of hexagonal honeycombs under axial and shear loading, part ii: Comparison of free skin and rigid skin effects on effective core properties. Mech Mater 2018;119:92–108.
- [33] Qiu K, Wang Z, Zhang W. The effective elastic properties of flexible hexagonal honeycomb cores with consideration for geometric nonlinearity. Aerospace Sci Technol 2016;58:258–66.
- [34] Zhao Y, Ge M, Ma W. The effective in-plane elastic properties of hexagonal honeycombs with consideration for geometric nonlinearity. Compos Struct 2020;234:111749.
- [35] Yang C, Moghaddam HS, Keshavanarayana SR, Horner AL. An analytical approach to characterize uniaxial in-plane responses of commercial hexagonal honeycomb core under large deformations. Compos Struct 2019;211:100–11.

- [36] Jiang Y, Wang Q. Highly-stretchable 3d-architected mechanical metamaterials. *Scientific Rep* 2016;6(1):1–11.
- [37] Bodaghi M, Damanpack A, Hu G, Liao W. Large deformations of soft metamaterials fabricated by 3d printing. *Mater Design* 2017;131:81–91.
- [38] Weeger O, Boddeti N, Yeung S-K, Kaijima S, Dunn ML. Digital design and nonlinear simulation for additive manufacturing of soft lattice structures. *Addit Manuf* 2019;25:39–49.
- [39] Restrepo D, Mankame ND, Zavattieri PD. Programmable materials based on periodic cellular solids. part i: Experiments. *Int J Solids Struct* 2016;100:485–504.
- [40] Restrepo D, Mankame ND, Zavattieri PD. Programmable materials based on periodic cellular solids. part ii: Numerical analysis. *Int J Solids Struct* 2016;100:505–22.
- [41] Rivello RM. *Theory and analysis of flight structures*. first ed. New York: McGraw-Hill; 1969.
- [42] Dawe D. *Matrix and finite element displacement analysis of structures*. Oxford, UK: Oxford University Press; 1984.